

Research on Channel Estimation and Interference Suppression in the OFDM Transmission System

August 2023

He He

Graduate School of
Science and Engineering

CHIBA UNIVERSITY

(千葉大学審査学位論文)

Research on Channel Estimation and Interference Suppression in the OFDM Transmission System

August 2023

He He

Graduate School of
Science and Engineering

CHIBA UNIVERSITY

Contents

Abstract	1
1 General Introduction	3
1.1 Background and Significance	3
1.2 Wireless Propagation and Fading	5
1.3 OFDM Scheme	7
1.4 Research directions in OFDM system	9
1.5 Research Focus of the Thesis	11
1.5.1 Channel estimation	11
1.5.2 IUI suppression	13
1.5.3 The relation of the thesis	15
2 Regression CNN based Fast Fading Channel Tracking using Decision feedback channel estimation	22
2.1 Introduction	22
2.2 Channel Model	26
2.3 Decision Feedback Channel Estimation (DFCE)	27
2.4 Conventional: GRNN-Based Channel estimation method using DFCE	28
2.4.1 Generalized Regression Neural Network (GRNN)	28
2.4.2 Conventional Scheme	31

2.5	Proposal: CNN-Based Channel estimation method using DFCE	33
2.5.1	DFCE channel image	33
2.5.2	Convolutional Neural Network	34
2.5.3	Regression CNN Based Channel Estimation	38
2.6	Computer Simulation	39
2.6.1	Simulation parameters	39
2.6.2	Regression CNN Trainings	41
2.6.3	Simulation Results	42
2.7	Conclusion	47
3	Data-aided weight with subcarrier grouping for Adaptive Array	
	Interference Suppression	51
3.1	Introduction	51
3.2	System model	54
3.2.1	Channel model	54
3.2.2	Uplink Array Antenna System Model	55
3.2.3	SMI Algorithm	56
3.2.4	Adaptive Subcarrier Grouping (ASG)	56
3.3	Proposal: Subcarrier grouping with data-aided weight	58
3.3.1	Initial Weight Calculation	59
3.3.2	Data-aided Weight Calculation	61
3.4	Computer Simulation	63
3.4.1	Simulation Parameters	63
3.4.2	Simulation Results	63
3.4.3	Computation Complexity	65
3.5	Conclusion	67
4	Conclusion	73

Acknowledgments	76
List of Related Papers	78

Abstract

With the improvement of the Internet of Things (IoT), a significant increase in transmission rate and the realization of huge system capacity is essential for the fifth generation of mobile communications (5G) and even beyond. To address this challenge, channel estimation and user interference mitigation are critical issues for the next generation of mobile wireless communication systems, including Orthogonal Frequency Division Multiplexing (OFDM) systems with high spectral efficiency and robustness against frequency-selective fading. For channel estimation, in high-speed mobility scenarios, channel state information (CSI) estimated at the beginning of the packet (the first OFDM symbol) is quite different from the last part because the actual channel state changes with time. Therefore, the channel estimation accuracy is degraded, leading to decreased communication performance. Many methods use more pilot symbols to overcome this problem. However, it leads to a decrease in the channel transmission efficiency. In addition, inter-user interference (IUI) greatly impacts the performance of the system. Beamforming technology is used as a solution to eliminate IUI. The Sample Matrix Inversion (SMI) method is a well-known weight estimation technique for antenna arrays used in beamforming. However, this method involves weight calculations for each subcarrier in OFDM systems, which poses challenges regarding interference suppression performance and computational complexity.

This thesis focuses on investigating the above important topics in OFDM systems with two methods: machine learning-based channel estimation and data-aided weight for interference suppression. The first method aims to improve channel estimation accuracy in high-mobility scenarios with low transmission efficiency. Conventional estimation methods, such as decision feedback channel estimation (DFCE) and DFCE-based GRNN estimation methods, can result in estimation errors due to the decision-making process when time and frequency-selective fading occurs. We focused on the time-frequency domain response of the CSIs, which can be represented as a two-dimensional image. Therefore, we newly propose a regression convolutional neural network (CNN) based channel tracking scheme using the time-frequency domain response of the CSIs by DFCE for training and prediction to solve these problems. Computer simulation results demonstrate that the proposed scheme can achieve higher BER performance and better processing time than the conventional schemes, and it is confirmed that the proposed method is effective even in high-speed environments. The second method is to improve the array weight to eliminate IUI by increasing the number of samples. As a conventional method, the adaptive subcarrier grouping (ASG) for SMI-based adaptive arrays has been previously proposed. However, this method needs to know the signal-to-noise ratio (SNR) in advance to set the threshold, perform grouping, and take the average, causing an insufficient number of signal samples. As a result, the ability to eliminate IUI is limited. To overcome this problem, we propose a new method based on data-aided weight calculation and the least mean square (LMS) algorithm by increasing the time domain samples without SNR. The decision results and initial weight are obtained by the SMI method with subcarrier grouping. Then the LMS method with subcarrier grouping is applied to reduce the weight estimation error and the amount of computation. Simulation results demonstrate that the proposed scheme is an efficient approach to improving BER performance under various Rician K factors.

Chapter 1

General Introduction

1.1 Background and Significance

The modern information society relies heavily on wireless communication systems, which have transformed how people connect and communicate. These systems have enabled the exchange of data and information across vast distances without physical connections, thereby revolutionizing how people and businesses communicate and operate. Among the various types of wireless communication systems, mobile wireless communications have undergone a rapid and dramatic evolution over the course of the last centuries [1].

In the 1980s, the first generation of the cellular network (1G) was first introduced and it mainly enabled voice services by using frequency division multiple access (FDMA). It can allow multiple users to communicate simultaneously by allocating different frequencies to each user. With the introduction of cellular systems and other groundbreaking technologies, 1G laid the foundation for the future of wireless communication, but it relied on analog technology.

During the 1990s, the advent of the second-generation mobile communication system (2G) marked a turning point in digital wireless communication. This new

technology adopts time division multiple access (TDMA) which enables data coding and compression and can offer high-quality global voice roaming service with high resolution. Since TDMA allows users to be assigned slots separated by time on the same frequency, it can improve the efficiency of spectrum utilization.

In the 2000s, The third-generation mobile communication system (3G) was launched. It employed a special coding scheme which is called code division multiple access (CDMA) to distinguish between users. It provided an information transfer rate of at least 144 kbit/s (high-speed motion), 384kbit/s (low-speed motion), and 2kbit/s (stationary). As a result, it achieved high-speed and high-capacity communications.

In the 2010s, the fourth generation (4G) of mobile communication systems was made accessible to consumers. It used orthogonal frequency-division multiple access for the downlink and single-carrier FDMA for the uplink to conserve power. In addition, it is based on long-term evolution(LTE) and provides a maximum downlink speed of 300 Mbit/s and a maximum uplink speed of 75 Mbit/s.

The fifth-generation mobile communication system (5G) is the newest technology standard for high-speed cellular networks in the telecommunications industry. It was first rolled out globally in 2019 and offers significant improvements in terms of connectivity speed and reliability. It required a peak download speed of 20 Gbit/s per second and 10 Gbit/s per second upload speed [2]. Therefore, the advancement and implementation of technologies to meet the ultra-high-speed and low-latency communication requirements of 5G evolution are currently in progress, as 5G is anticipated to be the fundamental technology for the future information society.

The above development courses of the world for mobile communications is shown in Fig.1.1.

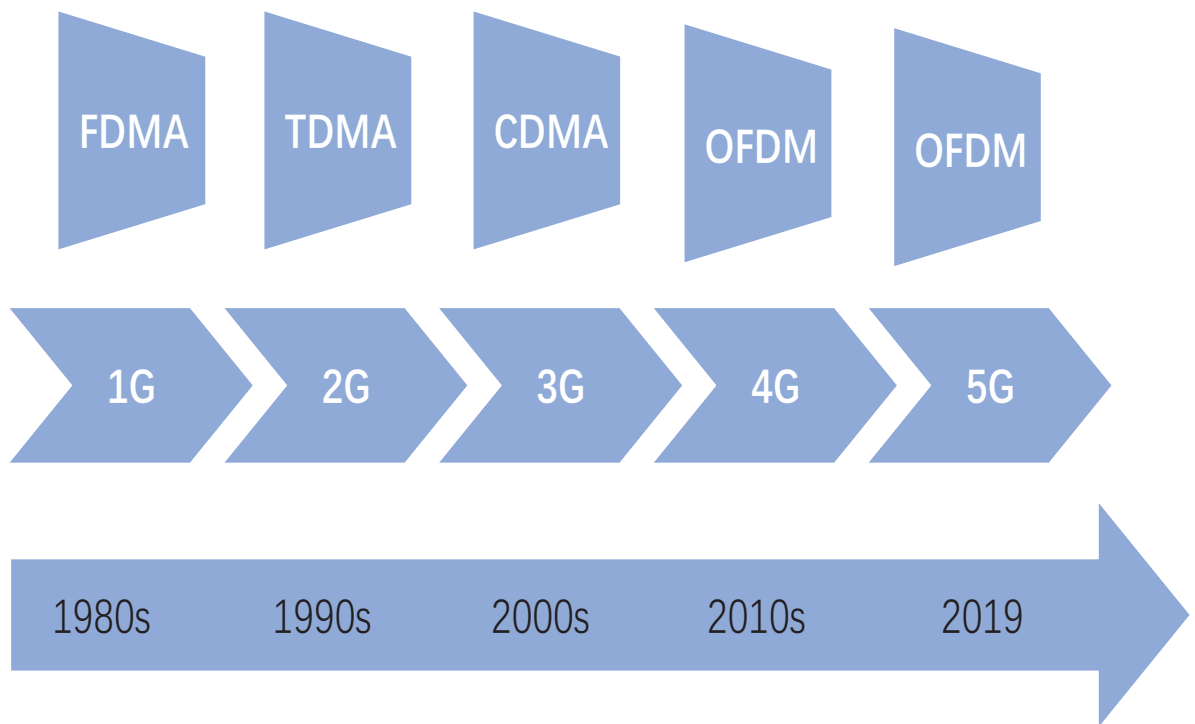


Figure 1.1: Development courses of world’s mobile communications.

1.2 Wireless Propagation and Fading

The wireless transmission channel is highly dynamic and unpredictable, so obtaining a precise estimation of the wireless channel characteristics becomes challenging. In fact, it is necessary to know the exact channel to achieve a high-quality wireless transmission system. The process of radio propagation for wireless communication has three fundamental physical transmission phenomena: reflection, diffraction, and scattering [3], shown in Fig.1.2. Reflection takes place and causes the transmitter power to be reflected back to its initial path when a radio wave encounters an obstacle that is much larger than the wavelength of the radio wave. Diffraction occurs when the path of a radio wave strikes the edge of a thin barrier or a surface with sharp bumps or small openings. Scattering is the physical phenomenon that occurs

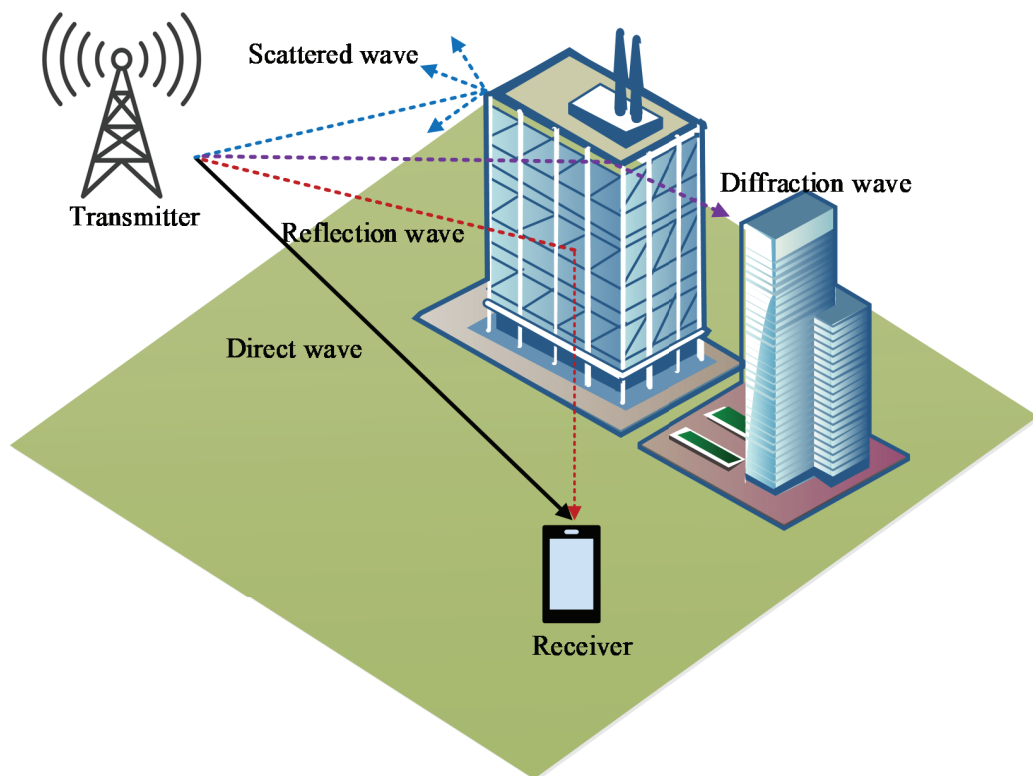


Figure 1.2: The radio propagation model.

when a radio wave collides with many particles with dimensions much smaller than the transmission wavelength. The propagation path loss of radio signals emanating from base stations is greatly affected by geographic terrain [4]. The signal can propagate over a greater distance when the base station is located at a higher elevation or further away from obstacles like trees or buildings. Radio wave propagation is extremely complicated, sensitive to terrain, and susceptible to reflection, diffraction and scattering, which can cause severe signal attenuation. The propagation of radio waves is also influenced by frequency; as frequency increases, path loss increases and the range of propagation distance decreases [5].

Fading is a phenomenon where the amplitude and phase of a non-additive signal vary with time and frequency. When scattered waves are present, the fading is

known as Rayleigh fading, while fading that consists of both scattered and direct waves are called Rician fading. The fading phenomenon in wireless communication can be classified into two categories: large-scale fading and small-scale fading. Large-scale fading consists of the shadowing of obstacles that affect the propagation of the transmitted waves, as well as the path loss as mobile objects move over large distances. By contrast, small-scale fading is a rapid variation in signal strength over short distances caused by multipath propagation. Multipath fading is categorized into flat fading and frequency-selective fading based on the signal and channel bandwidths. In flat fading, the transmission channel is much wider than the bandwidth of the transmitted signal. It causes all frequency components of the signal to be affected nearly uniformly. In contrast, frequency-selective fading is a phenomenon where the transmission of a signal with a wide bandwidth causes variations in the affected frequency components. Therefore, the wider the bandwidth of the transmitted signal, the more susceptible it is to frequency-selective fading. Meanwhile, temporal changes can be classified as fast fading and slow fading. They are distinguished by the speed of signal magnitude and phase change. Slow fading occurs when the coherence time of a channel is considerably longer than the delay, and the signal changes slowly over time. Conversely, fast fading causes the signal to fluctuate quickly over a short period of time when the channel's coherence time is significantly shorter than the delay.

1.3 OFDM Scheme

The demand for high-speed and high-capacity transmission has recently increased significantly, leading to a growing need for wideband communications. However, the transmission of a broadband signal, as mentioned in the previous section, is susceptible to frequency-selective fading caused by the multipath delay. The waveform

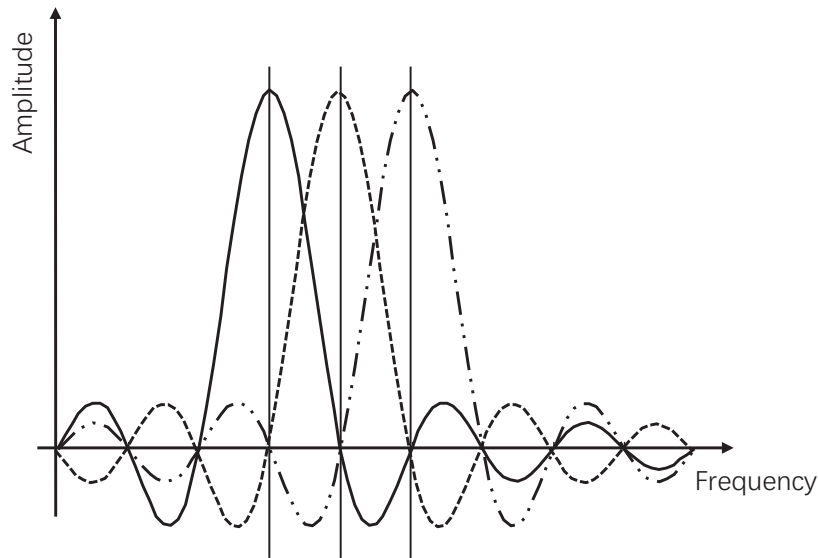


Figure 1.3: The orthogonality of OFDM

distortions and inter-symbol interference (ISI) can severely impact the accuracy of the decoded signal. Thus, addressing these issues is critical to ensure reliable communication in the wideband transmission system. OFDM (Orthogonal Frequency Division Multiplexing) is one of the solutions and widely used in wideband transmission [6].

OFDM is a type of digital signal modulation method that converts data into narrow-bandwidth data and arranges each subcarrier orthogonally to each other for parallel transmission in the frequency domain. The concept of OFDM is shown in Fig.1.3. Specifically, multiple input symbols are transformed into the time domain by performing an inverse fast discrete Fourier transform (IFFT). The transformed signal is then modulated by the carrier and sent from the transmitter side after the insertion of a guard interval (GI). The received signal removes the GI, which is then demodulated by the fast Fourier Transform (FFT) to recover the original symbols at the receiver. OFDM achieves higher spectral efficiency compared to conventional multi-carrier modulation methods by utilizing orthogonal carrier frequencies that

eliminate the need for guard bands between them [7]. This is because the orthogonalization allows the center frequencies of each subcarrier to overlap such that the signal strength of the other subcarriers is located at a null point in Fig.1.3, which can be easily extracted for separation without causing intercarrier interference. Furthermore, the serial-to-parallel conversion process performs high-speed data sequences, and a lot of subcarriers are used for low-speed parallel transmission. Due to the low speed of these carriers, the effect of delay spread becomes minimized. Although the effect of ISI could be reduced by adding GI into every OFDM symbol which is longer than the delay spread (e.g., add zero), the intercarrier interference (ICI) problem must also be considered. To suppress ICI and maintain orthogonality between carrier frequencies, GI is used as a cyclic prefix approach [8] where a portion of the OFDM symbol is replicated in the GI. Because of that, the sampling process can be in one complete cycle, and the orthogonality between carrier frequencies is maintained after demodulation, allowing for high-quality communication. Therefore, despite multipath time delays, OFDM can resist interference in wideband transmission while high-frequency efficiency can be maintained.

1.4 Research directions in OFDM system

Since OFDM transmission technology can transform a frequency-selective broadband channel into multiple flat narrowband channels, the channel can resist multipath propagation. In addition, OFDM can be easily combined with multiple antenna techniques to improve communication capacity. Because of its excellent performance, high flexibility and simple implementation, OFDM is expected to be continued as the basis for the next generation of communication standards (Beyond 5G). Therefore, it is always a hot research topic. The research directions for OFDM systems are shown below,

1. Channel estimation: Channel estimation is to determine the channel state information (CSI) between the transmitting and receiving antennas. At present, channel estimation methods can be divided into two types: One approach is using training sequences or pilot-based methods, which can be employed for the time-selectivity of the channel [9]. However, this method reduces the transmission efficiency due to the consumption of channel resources. The other one is blind channel estimation. Blind channel estimation uses statistical information to obtain the channel parameters to estimate the channel. It has high transmission efficiency because it does not occupy data resources. However, it has the problem of poor robustness and slow convergence. In addition, semi-blind channel estimation combining the above two methods has become the mainstream method recently.

2. Inter Carrier Interference (ICI) cancellation:

Due to problems such as carrier offset, orthogonality between subcarriers is lost, and ICI problem is incurred. ICI self-cancellation with windowing, parallel interference cancellation (PIC), and successive interference cancellation (SIC) as solutions are used for ICI cancellation [10]-[12]. It is worth noting that these methods can be combined with other signal processing methods to improve ICI cancellation performance. For example, windowing can be combined with SIC or PIC to improve ICI cancellation. In particular, windowing with SIC can reduce the ICI effect with lower complexity by concentrating the ICI effect and determining the number of dominant ICI terms [12].

3. IUI suppression: The IUI problem arises in a cellular network when multiple users exist. In this situation, it leads to signal overlap and interference, which makes it difficult for receiving side to separate and decode information from each user. This problem is typically caused by multiple users simultaneously using the same frequency on the wireless channel. Beamforming techniques can be employed to mitigate the IUI problem [13]. Beamforming utilizes adaptive array antennas to

control the direction of transmitted signals [14], focusing the signals in the desired direction and reducing interference while improving signal quality. However, some methods in this technique, such as SMI (Sample matrix inversion), incur computational complexity problems in OFDM systems due to the presence of subcarriers.

1.5 Research Focus of the Thesis

Over the past two decades, OFDM has been a heavily researched topic in communication systems due to its advantages in high spectral efficiency and robustness to frequency selective fading. However, this thesis will focus on discussing two major topics: improving channel estimation accuracy and mitigating IUI with low complexity.

1.5.1 Channel estimation

Since the transmitted signal is affected by the channel, the recovery of transmitted data requires the estimation of channel state information (CSI) at the receiver side. In general, OFDM systems often use pilot symbols to estimate the CSI of these specific frequencies and recover the transmitted signal. These pilot symbols are considered as known symbols and transmitted at regular intervals. On the receiver side, CSI can be obtained using different estimation methods. The Least Squares (LS) Estimation method [15] estimates the CSI by minimizing the squared errors between the received and estimated signals. In the Minimum Mean Squared Error (MMSE) Estimation method, it is similar to LS estimation but takes into account the noise variance in the received signal. In the Maximum Likelihood (ML) Estimation method [16], the CSI is estimated by maximizing the likelihood function of the received signal given the transmitted signal and the channel response. In addition, it has high computational complexity. The block-based estimation method is to

divide the frequency band into blocks [17]. Since the CSI of each block is estimated individually, this reduces the computational complexity of the estimation process. Compressed sensing (CS) estimation methods [18] use sparse signal processing to estimate the channel response. By exploiting the sparsity of the channel response, CS can estimate the channel response with a small number of pilot signals. However, additional channel sparsity needs to be known and has a high computational complexity to recover the signal. Among the above methods, we use LS as the basis for the discussion in this thesis since it has the lowest computational complexity and does not require additional conditions.

In a high-speed moving environment, the actual channel fluctuates over time, which causes large channel time variations in packets (symbols). The time variation in packets is shown in Fig.1.4. Therefore, different from the static environment, the impact of these changes cannot be ignored. Since the CSI in the last part of the packet differs from the one in the beginning part, the pilot estimated channel does not adequately track the temporal fluctuations of the channel, especially at the back of a packet. Therefore, Decision directed channel estimation (DDCE) has been proposed to overcome this problem [19]. In this method, detected symbol feedback is used to track the channel variation.

The receiver makes a decision based on the received signal and feeds the estimated signal back to the channel estimation algorithm, thus continuously updating its estimate of the channel. The algorithm updates the estimated channel based on the difference between the estimated signal and the received signal. This technique is performed repeatedly, with each iteration improving the accuracy of the estimated channel. The advantage of DDCE is that it does not require any prior knowledge of the channel characteristics. Since the receiver can adapt to the channel in real time based on feedback, it is particularly useful for the time-varying channel.

However, the performance of the DDCE method depends on the accuracy of the

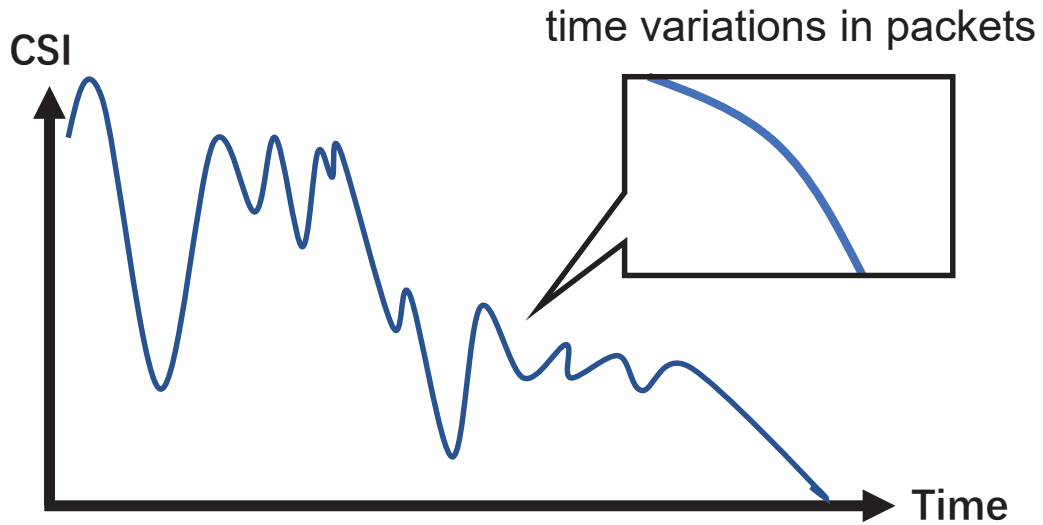


Figure 1.4: time variations in packets

decision. If the channel changes very fast over time, the accuracy of the channel estimation for the behind part of the symbols will be significantly degraded. In addition, repeated iterations can dramatically increase the computational complexity. Therefore, high-accuracy channel estimation with low computational complexity is critical and challenging in next-generation mobile communications.

1.5.2 IUI suppression

Inter-user interference (IUI) suppression is a vital challenge for mobile communication systems. When two users are in the same band at the same time, the transmission of one user can seriously affect the signal quality of the other user in the same band. At this time, inter-user interference occurs. This interference can result in significant degradation of data rates, which can negatively impact the user experience. Therefore, mitigating inter-user interference is particularly challenging in congested communication environments where multiple users share the same frequency band.

To overcome this problem, adaptive antenna array technology is one of the solutions to reduce the IUI problem, as shown in Fig. 1.5. Antenna arrays are composed of multiple antennas that are designed to receive or transmit signals in several directions at the same time. Antenna arrays can provide spatial filtering to improve the signal interference plus noise ratio (SINR) and reduce the effect of inter-user interference [20]. By using the antenna array, the desired signal can be separated from the interference signal, which can greatly reduce the impact of IUI on the received signal. Antenna arrays can also increase the system capacity and improve the overall performance of the wireless communication system. Moreover, the above antenna array is required in combination with adaptive signal processing, such as beamforming, which can maximize the optimization of transmission parameters and mitigate the impact of inter-user interference [21]. In other words, the implementation of adaptive techniques in array antennas can lead to significant improvements in the overall performance of wireless communication systems.

The adaptive signal processing in the OFDM-based system can be classified as the pre-FFT method in the time domain and the post-FFT method in the frequency domain [22]. In the pre-FFT method, the received signals of each element of the antenna array are combined before FFT processing. On the contrary, the post-FFT method is that the received signals of each element are processed by FFT processing before subcarrier combining by subcarriers. Although the Pre-FFT method has low operational complexity, the ability for IUI suppression is poor due to one-time signal processing, which dramatically affects communication performance. Therefore, the post-FFT method is usually adopted in the OFDM system.

The minimal mean square error (MMSE) adaptive array based on sample matrix inversion (SMI) is a powerful adaptive signal processing method to suppress IUI [23]. The SMI method uses frequency-domain signals for each subcarrier in OFDM to perform user separation by calculating the channel response from the

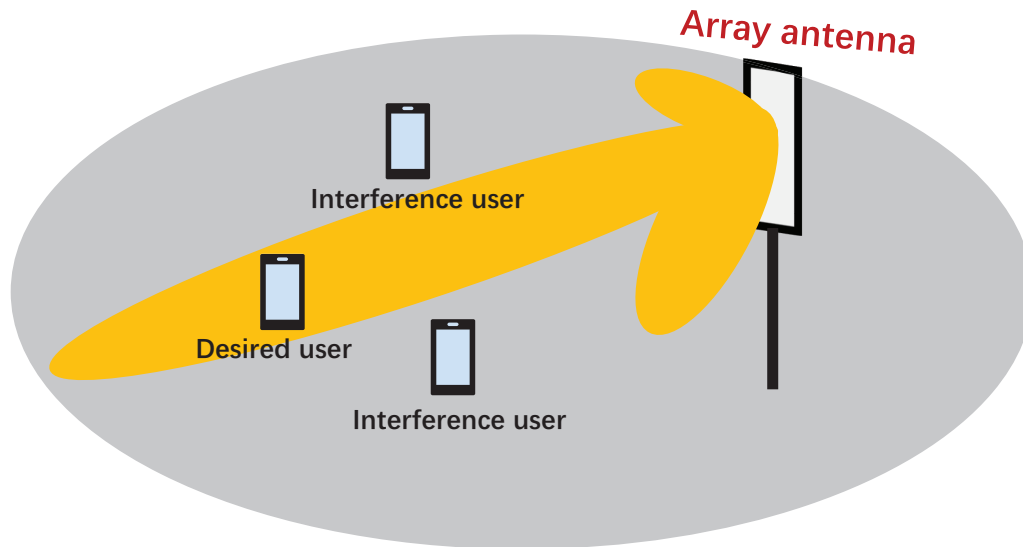


Figure 1.5: Antenna arrays for the IUI problem

correlation between known pilot symbols and the received signal. However, the SMI method uses a small number of samples when obtaining the covariance matrix, which degrades system performance. In addition, it is necessary to calculate weights for each subcarrier, which requires an enormous amount of computation. Low computational effort as well as high precision weights, are essential for the IUI problem in the adaptive array antenna.

1.5.3 The relation of the thesis

In recent years, the development of mobile wireless communication has led to the advancement of the Internet of Things (IoT) and autonomous driving and has further promoted the development of the information society. Therefore, wireless communication is one of the essential technologies for nowadays information society, and the demand for highly reliable communication technologies is unlimited. In order to achieve highly reliable communication, it is necessary to provide stable communication in various environments. It includes high-speed moving environments or

situations where there is interference from many users. Therefore, various methods are required to improve communication performance in different environments.

The focus of this research is channel estimation and IUI suppression in wireless communication to investigate two methods for different communication environments, respectively: one is to use machine learning to improve the accuracy of channel estimation under a high-speed mobile environment; the other is to expand the number of the samples in the frequency and time domains, which can improve the weight accuracy for IUI suppression with reducing the computational cost.

In Chapter 2, a regression convolutional neural network (CNN) based channel estimation method using the CSIs estimated by DFCE is proposed. In the fast-fading environment, the channel state information (CSI) in the last part of the packet is so different from the actual channel in the beginning part. Therefore, it is important to accurately estimate the actual CSI transition to improve the channel compensation capability. To overcome this problem, a GRNN-based channel compensation method has been proposed previously. This method uses the time domain training set to nonlinearly estimate the entire channel state transition. The training set is obtained from only the CSIs estimated by DFCE at the beginning of the packet. However, due to decision errors, DFCE sometimes provides inaccurate estimates of the channel state in the data symbols, especially in the behind part. Since the CSIs in the frequency domain are also correlated, time-frequency domain data is used to improve the accuracy of the training set. In addition, the utilization of regression CNN has higher generalization than GRNN, which makes the channel estimation accuracy much higher than GRNN. The simulation results show that the proposed method has better BER performance than the conventional methods.

In Chapter 3, a novel data-aided weight with subcarrier grouping for adaptive array antenna is proposed to suppress the IUI. To overcome the IUI problem, a well-known method for adaptive array interference suppression, the SMI method,

has been proposed. The accuracy of the weights is decreased due to the lack of sufficient samples, and the computational complexity is high due to the weights being calculated separately. An adaptive subcarrier grouping (ASG) method has been proposed to solve the above problem. In this method, subcarriers corresponding to similar fading are grouped and the group sizes are adaptively adjusted. On account of a scarcity of signal samples available within the confined set of pilot symbols, the interference suppression performance is inadequate. And it must depend on the SNR, resulting in higher computational complexity. The data-aided weight calculation method with subcarrier grouping does not require SNR or other information. In this way, more accurate weight estimation is achieved by increasing the sample amount. Additionally, the LMS algorithm is employed to ensure convergence with low computational complexity while using the initial weights. The simulation results demonstrate that the proposed scheme is an efficient approach and improves BER performance.

Finally, Chapter 4 concludes this thesis.

Bibliography

- [1] A. Osseiran, JF. Monserrat and P. Marsch, eds. “5G mobile and wireless communications technology,” Cambridge University Press, 2016.
- [2] A. Guntis, et al., “Spectrum considerations for 5G mobile communication systems,” *Procedia Computer Science*, vol.104, pp.509-516, 2017.
- [3] H. Bai and M. Atiquzzaman, “Error modeling schemes for fading channels in wireless communications: A survey,” *IEEE Communications Surveys and Tutorials*, vol. 5, no. 2, pp. 2-9, Fourth Quarter 2003. Doi: 10.1109/COMST.2003.5341334.
- [4] Lee, William CY. “Mobile communications engineering: theory and applications,” McGraw-Hill Education, 1998.
- [5] S. Sun et al., ”Investigation of Prediction Accuracy, Sensitivity, and Parameter Stability of Large-Scale Propagation Path Loss Models for 5G Wireless Communications,” *IEEE Transactions on Vehicular Technology*, vol. 65, no. 5, pp. 2843-2860, May 2016. Doi: 10.1109/TVT.2016.2543139.
- [6] H. Schulze, Henrik, and L. Christian, “Theory and applications of OFDM and CDMA: Wideband wireless communications,” John Wiley and Sons, 2005.
- [7] P. Patil, M. R. Patil, S. Itraj and U. L. Bomble, ”A Review on MIMO OFDM Technology Basics and More,” 2017 International Conference on Current Trends

- in Computer, Electrical, Electronics and Communication (CTCEEC), Mysore, India, pp. 119-124, 2017. Doi: 10.1109/CTCEEC.2017.8455114.
- [8] P. Cheol-Jin, and I. Gi-Hong, "Efficient cyclic prefix reconstruction for coded OFDM systems." *IEEE Communications Letters*, vol. 8, no. 5, pp. 274-276, May 2004.
- [9] A. Ladaycia, A. Mokraoui, K. Abed-Meraim and A. Belouchrani, "Performance Bounds Analysis for Semi-Blind Channel Estimation in MIMO-OFDM Communications Systems," *IEEE Transactions on Wireless Communications*, vol. 16, no. 9, pp. 5925-5938, Sept. 2017.
- [10] P. Singh and O. P. Sahu, "An Overview of ICI Self Cancellation Techniques in OFDM Systems," 2015 *IEEE International Conference on Computational Intelligence & Communication Technology*, Ghaziabad, India, 2015, pp. 299-302.
- [11] A. F. Molisch, M. Toeltsch and S. Vermani, "Iterative Methods for Cancellation of Intercarrier Interference in OFDM Systems," *IEEE Transactions on Vehicular Technology*, vol. 56, no. 4, pp. 2158-2167, July 2007. Doi: 10.1109/TVT.2007.897628.
- [12] C. R. Sheu, J. W. Liu and C. C. Huang, "A Low Complexity ICI Cancellation Scheme with Multi-Step Windowing and Modified SIC for High-Mobility OFDM Systems," 2010 *IEEE 71st Vehicular Technology Conference*, pp. 1-5, 2010. Doi: 10.1109/VETECS.2010.5493826.
- [13] Q. Xu, C. Jiang, Y. Han, B. Wang and K. J. R. Liu, "Waveforming: An Overview With Beamforming," *IEEE Communications Surveys and Tutorials*, vol. 20, no. 1, pp. 132-149, Firstquarter 2018. Doi: 10.1109/COMST.2017.2750201.

- [14] A. Sharma, S. Mathur, "Performance analysis of adaptive array signal processing algorithms," IETE Technical review, vol.33, no. 5, pp. 472-491, 2016.
- [15] J. -C. Lin, "Least-Squares Channel Estimation for Mobile OFDM Communication on Time-Varying Frequency-Selective Fading Channels," IEEE Transactions on Vehicular Technology, vol. 57, no. 6, pp. 3538-3550, Nov. 2008. Doi: 10.1109/TVT.2008.919611.
- [16] Pei Chen and H. Kobayashi, "Maximum likelihood channel estimation and signal detection for OFDM systems," 2002 IEEE International Conference on Communications. Conference Proceedings. ICC 2002 (Cat. No.02CH37333), New York, NY, USA, pp. 1640-1645 vol.3, 2002. Doi: 10.1109/ICC.2002.997127.
- [17] M. Singh, M. Singh, and A. Goraya. "Block based channel Estimation Algorithms for OFDM-IEEE 802.16 e (Mobile WiMAX) system." International Journal of Computer Applications 975, p.8887, 2011.
- [18] X. He, R. Song and W. -P. Zhu, "Pilot Allocation for Distributed-Compressed-Sensing-Based Sparse Channel Estimation in MIMO-OFDM Systems," IEEE Transactions on Vehicular Technology, vol. 65, no. 5, pp. 2990-3004, May 2016. Doi: 10.1109/TVT.2015.2441743.
- [19] D. Shin, S. Suyama, H. Suzuki and K. Fukawa, "10 Gbps millimeter-wave OFDM experimental system with iterative phase noise compensation," 2013 IEEE Radio and Wireless Symposium, Austin, TX, USA, 2013, pp. 184-186. Doi: 10.1109/RWS.2013.6486682.
- [20] J. Koppenborg, H. Halbauer, S. Saur and C. Hoek, "3D beamforming trials with an active antenna array," 2012 International ITG Workshop on Smart Antennas (WSA), Dresden, Germany, 2012, pp. 110-114. Doi: 10.1109/WSA.2012.6181190.

- [21] T. Lin and Y. Zhu, "Beamforming Design for Large-Scale Antenna Arrays Using Deep Learning," in *IEEE Wireless Communications Letters*, vol. 9, no. 1, pp. 103-107, Jan. 2020. Doi: 10.1109/LWC.2019.2943466.
- [22] AM Mahros, I Elzahaby, MM Tharwat, "Beamforming processing for OFDM communication systems." *Proc. of INCT 2012*, 2012.
- [23] L. Yu, W. Liu and R. Langley, "SINR Analysis of the Subtraction-Based SMI Beamformer," *IEEE Transactions on Signal Processing*, vol. 58, no. 11, pp. 5926-5932, Nov. 2010. Doi: 10.1109/TSP.2010.2058801.

Chapter 2

Regression CNN based Fast Fading Channel Tracking using Decision feedback channel estimation

2.1 Introduction

As the most widespread wireless communication method, packet-based transmission has been used. In this way, a transmitted data stream is separated into packets and the communication channel of each packet must be estimated to achieve correct signal recovery. Since the performance of the whole system depends on channel state information (CSI), it is crucial for communication performance improvement to find accurate CSI. Pilot-assisted channel estimation (PCE) [1] method is extensively used as one of the channel estimation (CE) methods. In this method, reference signals typically inserted at the beginning of the packet can estimate the CSIs in a static environment, such as Wi-Fi systems. However, it is difficult to compensate for the

amplitude and phase fluctuation in time-varying fading channels commonly associated with high-speed mobile systems. This is because the CSI estimated by the PCE is significantly different from the actual channel state, especially in the last part of the packet.

In order to solve this problem, several approaches have been proposed to trace the channel state transition. Data-aided decision feedback channel estimation (DFCE) has been proposed in [2], [3]. The DFCE uses the difference between the received symbols and the replica signal to estimate the channel variation corresponding to any given data symbol directly. The replica signal is calculated by multiplying the decision result of the transmitted signal by the CSI obtained by the PCE. In [4], linear model approximation in time-frequency blocks was proposed. [5] has proposed the comb-type pilot-aided channel estimation. However, these precedent channel estimation schemes cannot accurately estimate the channel with low computational complexity and fewer pilot signals under high Doppler frequency.

Recent advances in machine learning technology have enabled its application in several fields. There have been many studies using machine learning techniques to estimate CSI. Authors in [6] employed a fully connected neural network (NN) model for channel estimation and trained it for several subcarriers using simulated data. In [7], The authors propose a channel estimation network comprised of a convolutional neural network (CNN) and a bidirectional long short-term memory (BiLSTM) network, where the CNN is used to approximate frequency-domain interpolation processes and the BiLSTM network is utilized for time-domain channel prediction. However, there are still problems especially in real-time and high-speed mobile environments. Given the above background, a multilayer feedforward neural network (MLFNN) based channel estimation and compensation method has been previously proposed in [8], which is powerful even in high-speed environments. MLFNN with generalization capability is employed to compensate for the channel variation and

estimates the entire channel state transition. MLFNN is trained by partially obtained CSI by DFCE in the beginning part of the packet. Although it shows good tracking performance to cope with channel fluctuation, it needs improvement in estimation accuracy and computational complexity. Therefore, The improved version of this method was proposed to replace MLFNN with a generalized regression neural network (GRNN) [9]. Because of the one-pass learning process, the generalized regression neural network can remove the iterative training process with maintaining the generalization ability. The above methods demonstrate excellent channel tracking performance. However, the performance of the methods depends on the accuracy of the CSI used as training data. The estimated CSI by DFCE is sometimes incorrect due to decision errors even in the beginning part of the packet, when there is dramatic fluctuation in the channel state transition. For the above reasons, the estimator must decrease the disparity between data-aided CSIs and actual CSIs to further improve BER performance.

In order to solve these problems, we propose a channel estimation method based on supervised learning where a regression CNN is trained by the CSIs in the time and frequency domain. Since the DFCE method only considers temporal selectivity, the frequency selectivity of the data-aided CSIs is dispersed everywhere, in contrast to the continuously varying CSIs in neighbouring subcarriers. Therefore, errors of the DFCE can be effectively diminished by supervised learning, exploiting the two-dimensional information of CSIs in the temporal and frequency domains as a two-dimensional image. Since the two-dimensional information of CSIs has more complex characteristics than the one-dimensional one, it is difficult for the above NN to extract two-dimensional channel features and perform regression. That is why we apply CNNs, which have excellent feature extraction capabilities by performing convolution, pooling and connecting regression layers connected to two-dimensional input data. Because of the simultaneous processing of two-dimensional information

to correct the frequency-selective and time-selective data-aided CSIs, the estimation of the entire channel state transition could be more precise in a high Doppler environment. In addition, we trained the CNN using only the DFCE data under the high Doppler environment in the offline training process, and it is efficient under both high and low Doppler frequency in the offline estimation phase. Therefore, the proposed method does not require an additional estimator, such as a Doppler estimator, to track the time-varying channel. In summary, the major contributions of this paper are the following:

- (1) To mitigate the effects of erroneous CSI and reliably estimate the entire channel state transition even when data-aided CSI is inaccurate.
- (2) To obtain high channel estimation accuracy with limited pilot symbol even under a fast-moving environment.
- (3) To achieve generalization without requiring additional estimators, even in a lower Doppler environment.

In OFDM systems (Wi-Fi systems) based on the pilot structure set at the beginning of the packet, there have been few studies in recent years on tracking channel fluctuations in an extremely high-speed mobile environment. As an example, there is the reference [10] published in 2017. However, it has the limitation that only a Doppler shift of 8 km/h is used as a high-speed mobile environment (It corresponds to about $f_D = 37$ Hz if 5 GHz carrier frequency is assumed). On the other hand, the conditions targeted by our group are a Doppler frequency of 700 Hz, and especially in this paper, it is assumed to be 1000-2000 Hz. It achieves good BER performance under the most severe conditions, which is also acceptable for the millimeter wave band adopted in recent years. This is the first time such a performance has been achieved by applying machine learning, and it is our originality.

The rest of this paper is structured as follows. Section 2.2 denotes the channel model and OFDM system. Sections 2.3 and 2.4 introduce conventional methods.

Section 2.5 presents the proposed method. Simulation results are presented in Section 2.6. Finally, Section 2.7 concludes this paper.

2.2 Channel Model

In this paper, we assume Jakes' time-varying multipath fading channel, which is expressed as,

$$h(\tau, t) = \sum_{l=0}^{L-1} h_l(t) \delta(\tau - \tau_l), \quad (2.1)$$

$$h_l(t) = \frac{g_l}{\sqrt{Q}} \sum_{q=1}^Q \exp [j (2\pi f_D t \cos \alpha_q + \phi_q)], \quad (2.2)$$

where h_l and δ denote the complex channel coefficient and the Dirac 's delta function. τ_l represents the time delay of the l -th propagation path and there are L discrete paths in total. f_D denotes the maximum Doppler frequency. In addition, $2\pi f_D$ can be represented by the maximum Doppler radian frequency shift ω_D when $\omega_D = 2\pi f_D$. g_l , α_q and ϕ_q are the l -th path gain, angle of arrival of the q -th wave and its initial phase, respectively. The normalized path gain is assumed here as $\sum_{p=0}^{L-1} E [|h_l|^2] = 1$, where $E[\cdot]$ denotes the ensemble average operation. In non-line-of-sight (NLOS) communication, the probability density function of $|h_l|$ has Rayleigh distribution, as is widely known. Rayleigh fading is a type of multipath fading that contains this distribution characteristic. We can see from Eq. (2.2) that the channel coefficient contains a time-varying component, and the variation is magnified in a high-speed mobile environment. The frequency response $H(f, t)$ via Fourier transform of the temporal impulse response can be obtained as,

$$\begin{aligned} H(f, t) &= \int_0^{\infty} h(\tau, t) \exp(-j2\pi f\tau) d\tau \\ &= \sum_{l=0}^{L-1} h_l(t) \exp(-j2\pi f\tau_l), \end{aligned} \quad (2.3)$$

where f denotes the frequency. The frequency response is generally not flat in a mobile communication environment. $L > 1$ provides a frequency selective fading channel where the discrete expression of $|H(f, t)|$ varies. Due to this fading, the received signal level and phase components vary significantly in broadband transmission [11, 12].

2.3 Decision Feedback Channel Estimation (DFCE)

In this paper, single-input single-output based orthogonal frequency division multiplexing (SISO-OFDM) transmission is assumed. The pilot symbol is inserted into the first symbol of the packet, which can provide the reference CSI. The DFCE can use the demodulated signal and the CSI corresponding to the PCE to estimate the CSI of the data symbol [13]. The received signal corresponding to the m -th subcarrier and the n -th data symbol $Y(m, n)$ is expressed as,

$$Y(m, n) = H(m, n)X(m, n) + N(m, n), \quad (2.4)$$

where $H(m, n)$ represents the channel coefficient, i.e. $H(\frac{m}{T_d}, nT_s)$ in Eq. (2.4) where T_s and T_d denote the OFDM symbol duration and its effective symbol length without guard interval (GI). $X(m, n)$, and $N(m, n)$ indicate the transmitted symbol, and Additive white Gaussian noise (AWGN), respectively. The CSI $\tilde{H}(m)$ at the pilot symbol is obtained by dividing the received pilot symbol $Y(m, 0)$ by the transmitted pilot symbol $X(m, 0)$, as shown below.

$$\begin{aligned} \tilde{H}(m) &= \frac{Y(m, 0)}{X(m, 0)} \\ &= H(m, 0) + \frac{N(m, 0)}{X(m, 0)}. \end{aligned} \quad (2.5)$$

Then, the decision result of the transmitted symbol $\tilde{X}(m, n)$ is derived as below.

$$\tilde{X}(m, n) = \mathcal{D} \left[\frac{Y(m, n)}{\tilde{H}(m)} \right], \quad (2.6)$$

where $\mathcal{D}[\cdot]$ represents the decision function. The adjusted CSI at the n -th data symbol $\check{H}(m, n)$ is obtained by dividing the actual received signal $Y(m, n)$ by $\tilde{X}(m, n)$.

$$\begin{aligned}\check{H}(m, n) &= \frac{Y(m, n)}{\tilde{X}(m, n)} \\ &= H(m, n) \frac{X(m, n)}{\tilde{X}(m, n)} + \frac{N(m, n)}{\tilde{X}(m, n)}.\end{aligned}\tag{2.7}$$

Due to the existence of additive noise effects, The accuracy of the adjusted CSI is reduced and may lead to a decrease in demodulation accuracy. In order to mitigate the noise impact, the symbols of adjacent adjusted CSIs are averaged together, i.e. CSIs are calculated by averaging adjacent three samples [13] which denote $\check{H}(m, n - 1)$, $\check{H}(m, n)$ and $\check{H}(m, n + 1)$,

$$\hat{H}(m, n) = \frac{\sum_{k=n-1}^{n+1} \check{H}(m, k)}{3}.\tag{2.8}$$

However, decision errors are still unavoidable in this method resulting in inaccurate CSI estimation, as shown in Fig. 2.1. It is worth noting that in the high Doppler frequency shift environment, the channel changes from the CSI in the pilot symbol to the one behind is extremely significant, especially in the behind part of the data packet. That is why applying DFCE given by pilot-aided CSI in a fast-fading environment cannot fully improve the channel tracking performance.

2.4 Conventional: GRNN-Based Channel estimation method using DFCE

2.4.1 Generalized Regression Neural Network (GRNN)

GRNN has been used for the neural network portion to avoid the iterative training procedure while maintaining generalization capacity [14]. GRNN was proposed by Donald Specht in 1991, which evaluates the probability density function to solve

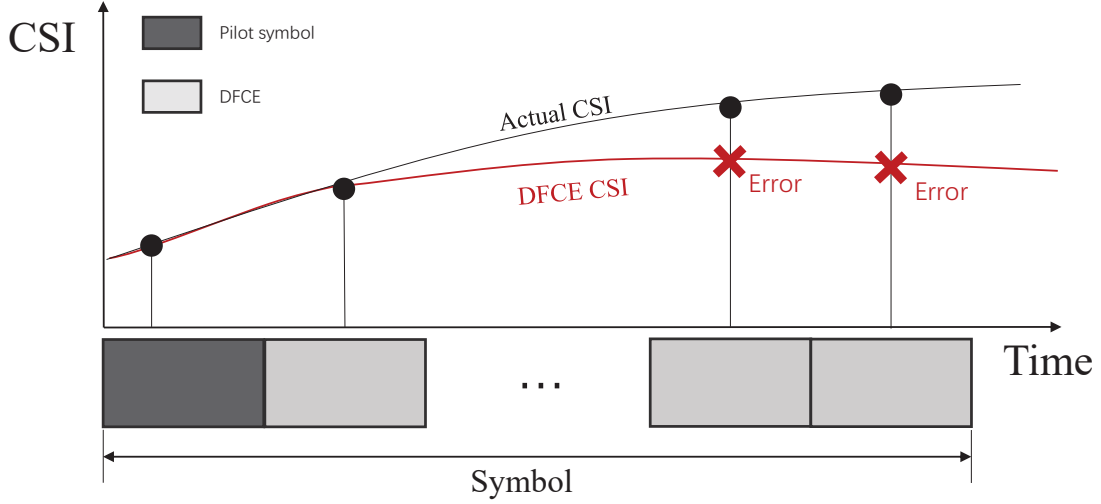


Figure 2.1: Actual CSI and DFCE CSI per subcarrier in the time variation

the nonlinear approximation problem [15]. GRNN has excellent performances in both robust function approximation ability and learning speed. This is because it can rapidly provide convergence to the optimal regression surface by using a probability distribution, even though the sparse training samples included inaccurate responses. Besides, GRNN directly sets weight values to training samples regarded as the expected response value. As shown in Fig. 2.2, the GRNN is a parallel four-layer structure: input layer, pattern layer, summation layer, and output layer [16].

The procedure for calculating the output values of the first output neuron is described below. $\mathbf{x} = [x_1, x_2, \dots, x_n]$ denotes the input vector. \mathbf{c}_i denotes the i -th training input vector ($1 \leq i \leq N_t$) where N_t presents the number of training sets. The output of the i -th neuron in the pattern layer is expressed as

$$\Psi_i(\mathbf{x}) = \exp\left(-\frac{(\mathbf{x} - \mathbf{c}_i)^2}{r^2}\right), \quad (2.9)$$

where r denotes the radius of the radial basis function (RBF). This parameter can determine the generalization capability of the GRNN by controlling the degree of smoothness. When r is large, the ability to approximate dispersed training samples

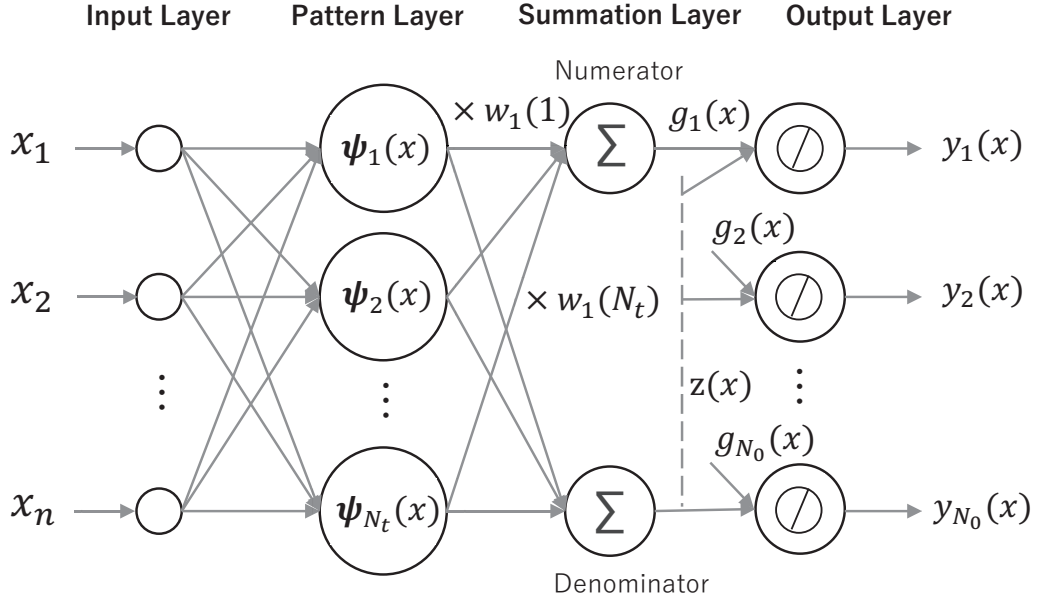


Figure 2.2: Architecture of GRNN.

decreases due to smoother transitions. In contrast, when r becomes very small, the regression curve will change rapidly, causing a decrease in the prediction ability.

The output of the i -th pattern neuron in the pattern layer is multiplied by the i -th desired response and then fed into the numerator neuron in the summation layer. As a result, the output of the numerator neuron $\mathbf{g}_1(\mathbf{x})$ is expressed as

$$\mathbf{g}_1(\mathbf{x}) = \sum_{i=1}^{N_t} w_1(i) \Psi_i(\mathbf{x}). \quad (2.10)$$

The output of the denominator neuron $\mathbf{z}(\mathbf{x})$ is expressed as

$$\mathbf{z}(\mathbf{x}) = \sum_{i=1}^{N_t} \Psi_i(\mathbf{x}). \quad (2.11)$$

From (2.10) and (2.11), the output of the first output neuron, $\mathbf{y}_1(\mathbf{x})$, is calculated as

$$\mathbf{y}_1(\mathbf{x}) = \mathbf{z}(\mathbf{x}) / \mathbf{g}_1(\mathbf{x}). \quad (2.12)$$

When the outputs in the pattern layer are seen as weights, as was previously explained, GRNN output indicates a weighted average of the required responses [17, 18]. By replacing \mathbf{g}_1 with \mathbf{g}_k and $w_1(i)$ with $w_k(i)$, the output of the k -th output neuron ($k = 1, 2, \dots, N_o$) can be calculated by using (2.9)-(2.12), where N_o represents the number of GRNN outputs.

2.4.2 Conventional Scheme

This paper describes channel tracking based on GRNN as a conventional scheme using CSI obtained through PCE and DFCE [14]. Because of the nonlinear generalization capabilities, GRNN can be trained by the estimated CSIs at the beginning and middle parts of the packet to trace the whole CSI transition accurately. In addition, this approach unnecessitates to repeat the iterative learning process. Fig. 2.3 shows the block diagram of channel estimation based on GRNN when the number of subcarriers is N_c . Each output of GRNN corresponds to the CSI at the m -th subcarrier ($m = 1, 2, \dots, N_c - 1, N_c$). In the GRNN method, the training inputs are the center of each RBF in the pattern layer and the desired responses are to be the weight of weighted summation directly in the summation layer. GRNN can predict an arbitrary function that relates an input vector to the desired responses by the training. During the GRNN training, the 1st desired response and the 2nd one are set as CSIs estimated by PCE for the 1st symbol and by DFCE for the 10th symbol, respectively. The indices [1, 10] can be defined as the training input. The reliability of the desired responses can be maintained by acquiring only the CSI estimated through DFCE in the beginning part of the packet. Then, every RBF centers on the pattern layer and multiplication values at nodes from the pattern layer to the numerator neurons are directly defined by the training input and the desired response, respectively. Finally, the vector containing indices for all data symbols $[1, 2, \dots, N_d]^T$ input the GRNN, where N_d is the number of data symbols.

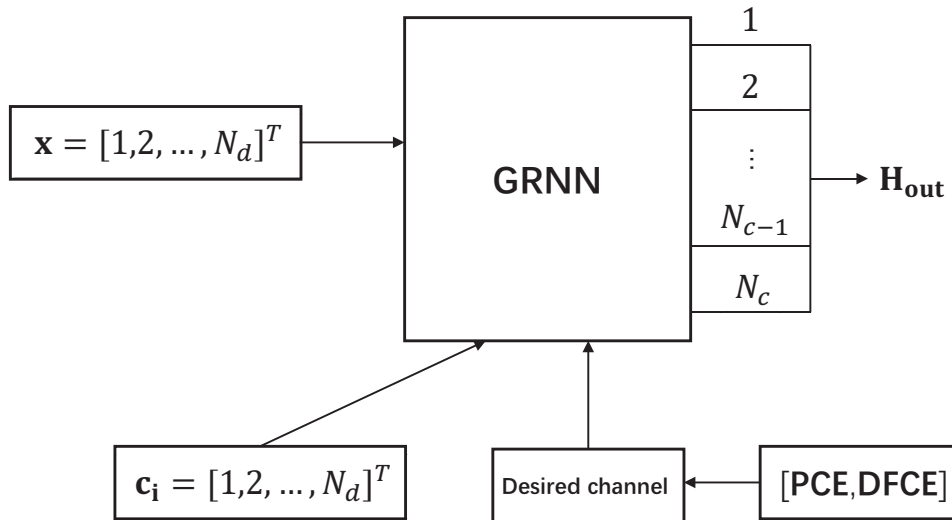


Figure 2.3: Block diagram of the GRNN-based channel estimation.

Consequently, GRNN outputs the entire channel state transition given by

$$\mathbf{H}_{\text{out}} = \begin{bmatrix} h_{\text{out}}(1, 1) & h_{\text{out}}(1, 2) & \cdots & h_{\text{out}}(1, N_d) \\ h_{\text{out}}(2, 1) & h_{\text{out}}(2, 2) & \cdots & h_{\text{out}}(2, N_d) \\ \vdots & \vdots & \ddots & \vdots \\ h_{\text{out}}(N_c, 1) & h_{\text{out}}(N_c, 2) & \cdots & h_{\text{out}}(N_c, N_d) \end{bmatrix}, \quad (2.13)$$

where $h_{\text{out}}(m, n)$ ($n = 1, 2, \dots, N_d$) is the estimated CSI by the trained neural network at the n -th data symbol and the m -th subcarrier.

However, in a fast-fading environment, the channel state transition is rapid, even in the beginning part of the symbol. This rapid transition can lead to inaccuracies in the CSI estimated by only DFCE due to decision errors, even when DFCE is performed at the beginning of the symbol. Therefore, it is difficult to achieve comprehensive performance improvements by focusing solely on the time domain, such as the GRNN-based channel estimation method using DFCE in the time domain. To fully enhance performance, considering other domains besides the time domain becomes necessary.

2.5 Proposal: CNN-Based Channel estimation method using DFCE

We propose a new method to estimate the whole CSIs using CNN trained by DFCE channel images. When frequency selectivity and significant time variation of CSIs exist, incorrect CSIs are generated by DFCE, causing severe performance degradation under a fast-fading environment. In particular, DFCE only considers the time domain response and the selective fading in the frequency domain is not considered. In addition, the time-frequency response of the CSIs can be considered as a two-dimensional image. Therefore, We employ the two-dimension image feature extraction and generalization capability of CNN to improve the low-quality channel estimation problem caused by DFCE. The flowchart of our channel estimation method using the proposed CNN-based method is shown in Fig. 2.4. The estimator composed of CNN is pre-trained offline and then utilized for online processing to track the rapidly changing channel. Finally, the received estimated CSIs are utilized to recover the received signal.

2.5.1 DFCE channel image

The complex-valued channel time-frequency domain response matrix $\hat{\mathbf{H}} \in \mathbb{C}^{N_d \times N_c}$ (the number of symbols is N_d and the number of subcarriers is N_c) between a transmitter and a receiver can be represented as two two-dimensional images [19], which are estimated by DFCE. One two-dimensional image represents the real part and another one represents the imaginary part. Preprocessing the complex-valued channel is critical for CNN in the next section. Figure. 2.5 illustrates the real part of two-dimensional time-frequency image for a sample estimated channel and an actual channel ($N_d = 20$ symbols and $N_s = 64$ subcarriers). As seen in Fig. 2.5(a), although in a high SNR environment, it is difficult to correctly estimate the actual channel

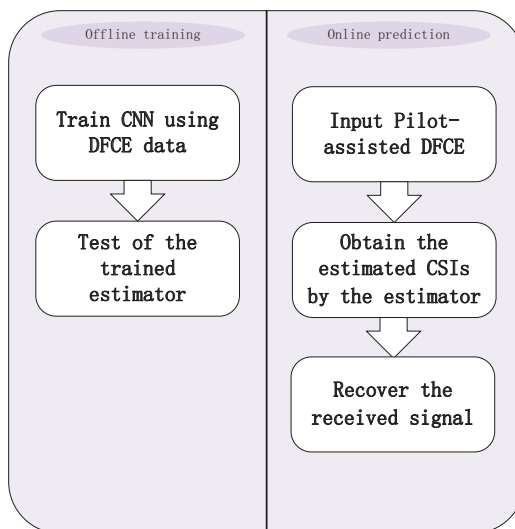


Figure 2.4: CNN structure of the proposed method.

due to the frequency selectivity of the subcarrier and the fast time variation of the channel.

2.5.2 Convolutional Neural Network

Convolutional neural network (CNN, or ConvNet) is a type of Artificial Neural Network (ANN) most frequently used in deep learning to evaluate visual imagery [20]. The proposed CNN consists of two parts: a feature extraction part and a regression part. The structure of the CNN is shown in Fig. 2.6. The first convolutional layer uses 64 kernels of size 5×5 in the filter and its output size is $64 \times 20 \times 64$; the second and third layer uses 32 kernels of size 3×3 , followed by ReLu activation. The fourth layer uses one kernel of size 3×3 . The output sizes are $64 \times 20 \times 32$, $64 \times 20 \times 32$ and $64 \times 20 \times 3$ in the second, third and fourth convolutional layer. The final layer is the regression layer used to calculate errors and reconstruct the images. Its output size is $64 \times 20 \times 2$.

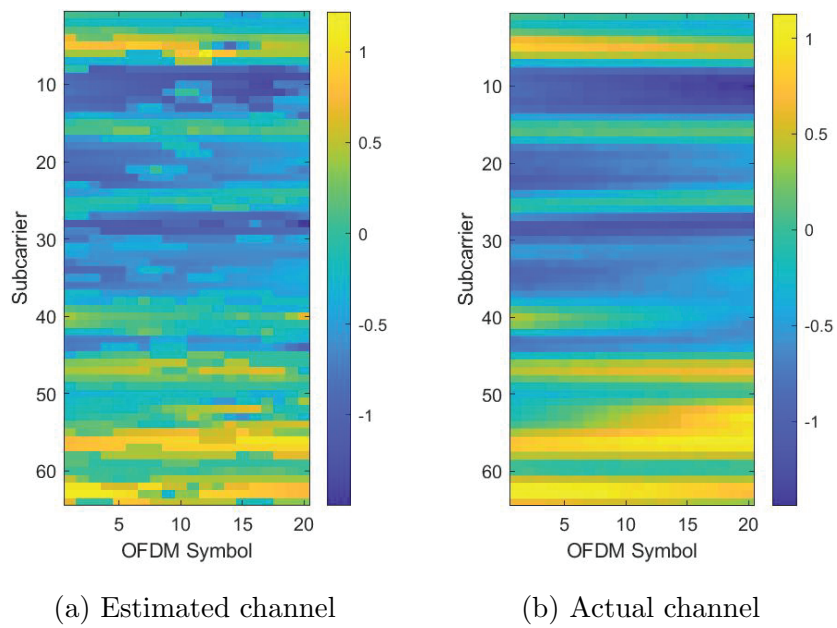


Figure 2.5: Estimated channel vs actual channel corresponding to the real part in frequency and time domain when SNR=30 dB, Doppler frequency =2000 Hz.

Specifically, the output of the $(l+1)$ -th convolutional layer is defined as

$$y_{u,c',p',q'}^{(l+1)} = \sum_{c=1}^C \sum_{i=1}^{K_h} \sum_{j=1}^{K_w} w_{c',c,i,j}^{(l+1)} \cdot x_{u,c,p,q}^{(l)} + b_{c'}^{(l+1)} \quad (2.14)$$

where $c(c = 1, \dots, C)$ and $c'(c' = 1, \dots, C')$ are the input and the output channel indices, respectively. $i(i = 1, \dots, K_h)$ and $j(j = 1, \dots, K_w)$ represent the height and the width of the kernel. $u(u = 1, \dots, U)$ is the index of mini batch. $x_{u,c,p,q}^{(l)}$ is the output of the element (p, q) in the u -th mini batch of the c -th channel on the l -th layer, $w_{c',c,i,j}^{(l+1)}$ indicate the weight at (i, j) position of the c -th channel and c' -th channel kernel on the $(l + 1)$ -th layer, and $b_{c'}^{(l+1)}$ denotes the bias of c' -th channel on the $(l + 1)$ -th layer. $y_{u,c',p',q'}^{(l+1)}$ is the output of the element (p', q') in u -th mini batch of c' -th channel on the $(l + 1)$ -th layer. (p', q') are represented as

$$\begin{aligned} p' &= P_h - i + p + 1 & (p' = 1, \dots, P'), \\ q' &= P_w - j + q + 1 & (q' = 1, \dots, Q'), \end{aligned} \quad (2.15)$$

where P_h and P_w are the paddings of height and width. The above parameters of the proposed CNN structure are shown in Table 2.1. The purpose of applying padding is to ensure consistency in size.

Table 2.1: Parameters of CNN structure

l	1	2	3	4
C	2	64	32	32
$K_h = K_w$	5	5	3	3
$P_h = P_w$	2	2	1	1

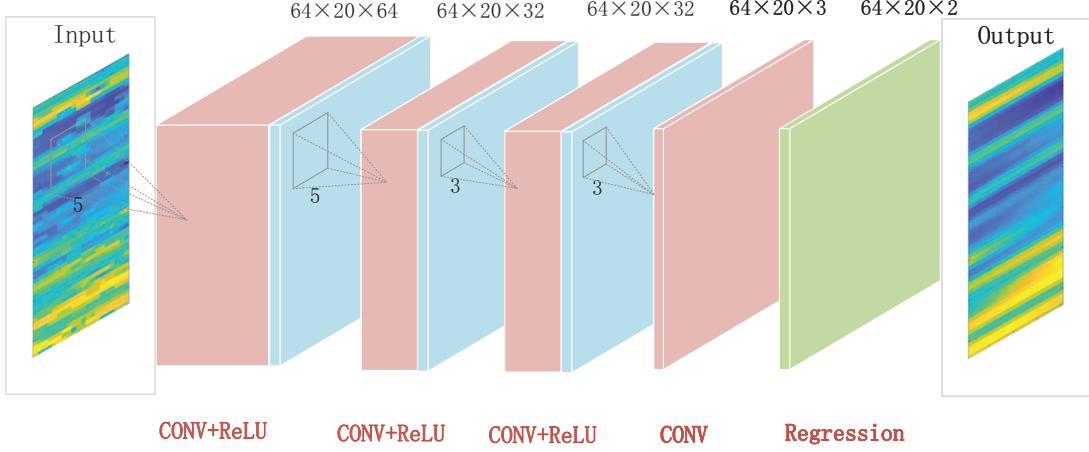


Figure 2.6: CNN structure of the proposed method.

After that, the output through the activation layer is expressed as

$$x_{u,c,p,q}^{(l+1)} = \max \left(0, y_{u,c',p',q'}^{(l+1)} \right). \quad (2.16)$$

It is the rectified linear unit (ReLU) used as an activation function. CNN feature extraction is carried out by repeating (2.14) to (2.16) before the last convolutional layer. The last convolutional layer does not perform (2.16). Finally, the loss function of the regression layer is the half-mean-squared-error between the output of the last convolutional layer and the two-dimensional desired response in the u -th mini batch calculated as follows:

$$loss = \frac{1}{2} \sum_{e=1}^{P' \cdot Q' \cdot C'} (y_{u,e}^{(l)} - d_{u,e})^2 \quad (2.17)$$

where the output tensor of the last convolutional layer $y_{u,e}$ and the desired response tensor $d_{u,e}$ are used to calculate each element ($1 \leq e \leq P' \cdot Q' \cdot C'$). In order to minimise the loss function, these weights and biases are updated using a back-propagation method [20].

2.5.3 Regression CNN Based Channel Estimation

First, we train the CNN offline using the estimated channel $\hat{\mathbf{H}}$ by DFCE and the assumed actual channel under the only high Doppler shift environment (i.e. Doppler frequency is 2000 Hz and the normalized value is 8×10^{-3}) as the training input and the desired response. By separating the real and imaginary parts of the CSIs, the training data becomes two two-dimensional images. For example, we input the real and imaginary part of one estimated CSI into the first layer ($l = 0$) of the CNN in the u -th mini batch as (2.14),

$$x_{u,1,m,n}^{(1)} = Re \left\{ \hat{H}(m, n) \right\} \quad (2.18)$$

$$x_{u,2,m,n}^{(1)} = Im \left\{ \hat{H}(m, n) \right\} \quad (2.19)$$

One assumed actual CSI \mathbf{H} is used to be the desired signal in the regression layer as (2.17), and the assumed actual channels are acquired in advance from all transmitted pilot symbols.

$$y_{u,1,m,n}^{(l)} = Re \left\{ H(m, n) \right\} \quad (2.20)$$

$$y_{u,2,m,n}^{(l)} = Im \left\{ H(m, n) \right\} \quad (2.21)$$

Therefore, the CSI estimated by CNN can be obtained in the next step.

Next, we estimate CSIs in the online stage. Figure. 2.7 illustrates the flowchart of channel estimation using the proposed CNN-based method. The goal is to estimate the channel state in the time-frequency domain using the transmitted pilots set at the beginning of symbols. We exploit the pilot signal set at the beginning of symbols to perform channel estimation at first. Then, the data-aided channel estimation is performed by DFCE using pilot-aided CSIs. The estimated channel by DFCE is input to the proposed CNN, which has been trained offline. In general, CNN comprises numerous parallel filters connected via a set of weights to a local patch of input data. In order to calculate the convolutional products, these filters traverse the

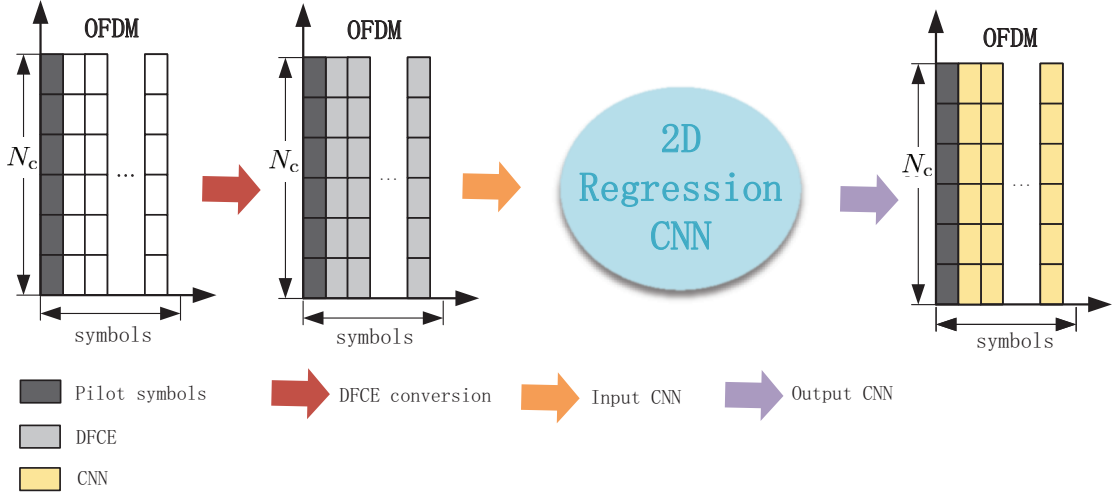


Figure 2.7: The data flow of the proposed Regression CNN

data in two dimensions, namely vertically and horizontally. In contrast to previous methods, the channel estimate errors caused by DFCE are mitigated by evaluating the relationship in both the time and frequency domain using the CNN filters. In other words, each weight w of the filters is shared in both the frequency and time domains from (2.14). Finally, the estimated channel output by the CNN is used to recover the received signal.

2.6 Computer Simulation

2.6.1 Simulation parameters

The simulation parameters are listed in Table 2.2. We use Convolutional codes ($R = 1/2$, $K = 7$) and the random interleaver for FEC in OFDM system with a bandwidth of 20 MHz [21]. The OFDM symbol duration T_s including guard interval (GI) is $4 \mu\text{s}$ (actual value) and its effective DFT symbol length T_d is $3.2 \mu\text{s}$, referred to the basic Wi-Fi specifications. In addition, we consider the ideal case, i.e., no null

Table 2.2: Simulation parameters

Transmission scheme	OFDM
Bandwidth	20 MHz
FFT size, Number of carriers	$N_c=64$
Guard interval	16
Number of pilot/data symbols	$N_p = 1, N_d = 20$
Channel model	15 path Rayleigh fading
Path interval	1
Max Doppler frequency	10, 1000, 2000 Hz $(f_D T_s = 4 \times 10^{-5}, 3.2 \times 10^{-3}, 8 \times 10^{-3})$
Data modulation	QPSK
Forward error correction	Convolutional code (FEC) $(R = 1/2, K = 7)$

subcarriers set (guard band). Null subcarriers will be considered in future work. The cyclic prefix (CP) is employed as guard interval (GI) and its number is 16. Moreover, the Jakes' fading model represents time-varying channel where there are 15 multipaths and the average path gain of each path is attenuated by 1 dB, as shown in Fig. 2.8. Here, the multipath delay interval is $0.05 \mu\text{s}$, which also means sampling time. In order to represent various scenarios of the transceiver moving

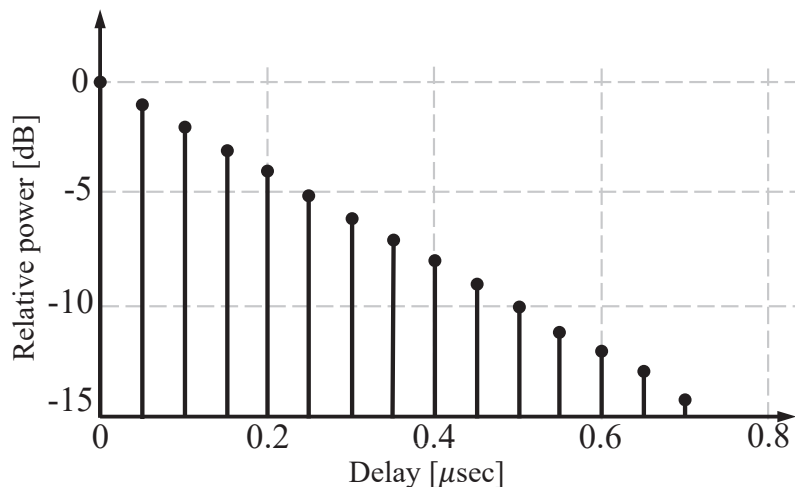


Figure 2.8: Channel model

environment, the maximum Doppler frequency is set to 10 Hz, 1000 Hz, and 2000 Hz, respectively. The normalized values $f_D T_s$ are 4×10^{-5} , 3.2×10^{-3} , 8×10^{-3} , respectively.

2.6.2 Regression CNN Trainings

The images of the DFCE channel and actual channel used for the simulation are $64 \times 20 \times 2$ in size, including the real and imaginary parts. All the images are generated using MATLAB R2021b. During the offline training phase, SNR is determined as 30 dB, and the maximum Doppler frequency is set to only 2000 Hz. We created a dataset of 10,000 received channels. The network is trained using the mini batch gradient descent method, with each mini batch size of 128. The optimizer uses the adaptive moment estimation (ADAM) algorithm. The initial learning rate is set to 8×10^{-4} , and the validation is implemented every 250 iterations. The network is trained on an NVIDIA GeForce GTX 1660 SUPER GPU with MATLAB Deep Learning Toolbox. The whole process of the simulation experiments is carried out on Windows 10 with an AMD Ryzen 5 3500 6-Core Processor CPU.

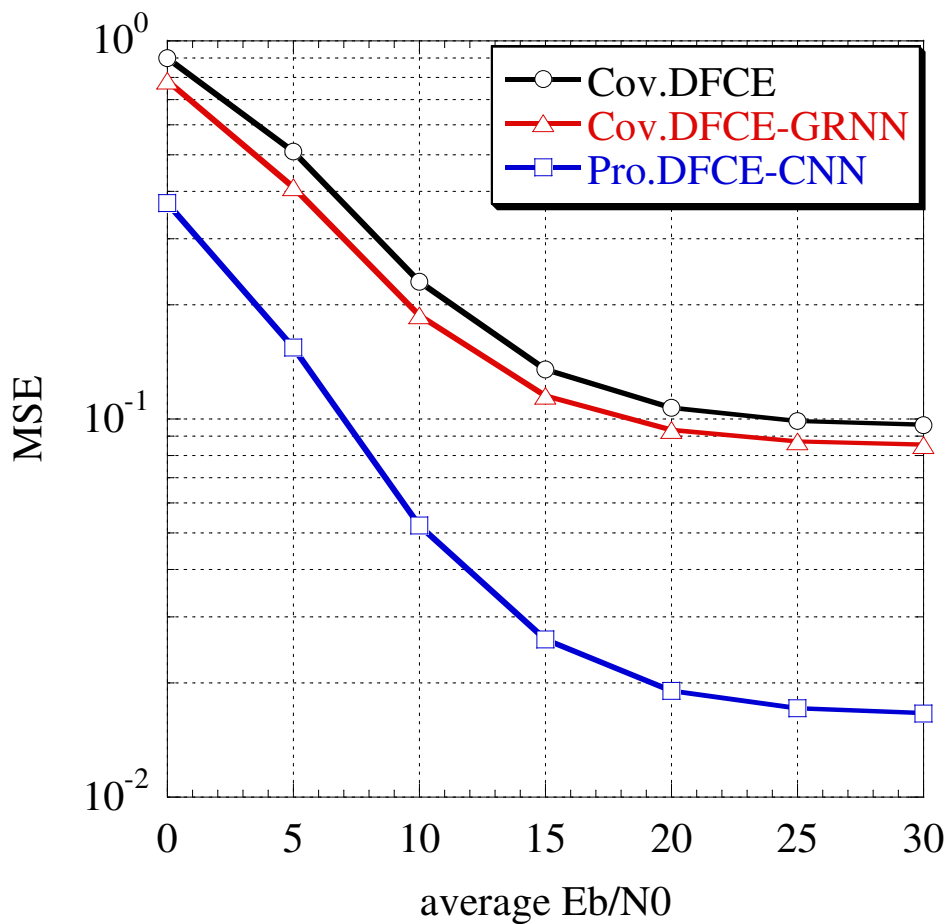


Figure 2.9: Mean square error for channel estimation.

2.6.3 Simulation Results

Figure. 2.9 compares the mean square error (MSE) for the DFCE only, the conventional GRNN method [8, 9] and the proposed channel estimation methods at a maximum Doppler frequency of 2000 Hz. MSE calculates the error using the actual CSI and the estimated CSI. It can be seen that the proposed method has the

best MSE for various SNR cases and the estimated CSI is the closest to the actual CSI. This is because the estimated CSIs by DFCE are compensated by CNN in the frequency and time directions in a lump sum, which can improve the estimation accuracy. In other words, the proposed method considers not only the time variation but also the relevance of the frequency selectivity. However, the GRNN method only uses the one-dimensional DFCE data to compensate for CSIs in the time direction, not considering the relevance of two-dimensional information.

Figure. 2.10 shows the BER performances of the conventional and proposed methods at a maximum Doppler frequency of 2000 Hz. The theoretical BER is calculated when the channel states for all data symbols are ideally known. Due to the fast time-varying channel, decision errors often occur in the last part of the packet, resulting in a significant deterioration of the BER performance of the DFCE. Although the conventional GRNN method can achieve slightly higher BER performance than DFCE-only, the error floor appears at around $\text{BER} = 10^{-1}$ and is almost as close to the DFCE-only case. The proposed method achieves the best BER performance below 10^{-1} and is the closest to the ideal case. This is because the proposed method has the lowest channel estimation error in the high Doppler environment, as shown in Fig. 2.9.

In summary, the proposed method improves channel estimation accuracy by CNN trained by two-dimensional DFCE data. Furthermore, although the offline training set of the proposed network is trained at SNR=30 dB only, the input signal in the low SNR case can also improve the performance due to partial noise reduction in the DFCE method and the generalization of the CNN. Furthermore, when the training sets consist of CSIs with high SNR, the CNN can extract complicated channel characteristics at high Doppler frequency shifts with greater accuracy.

In order to better demonstrate the universality of the proposed method, figure.2.11 shows the results at the maximum Doppler shift of 1000 Hz and 10 Hz,

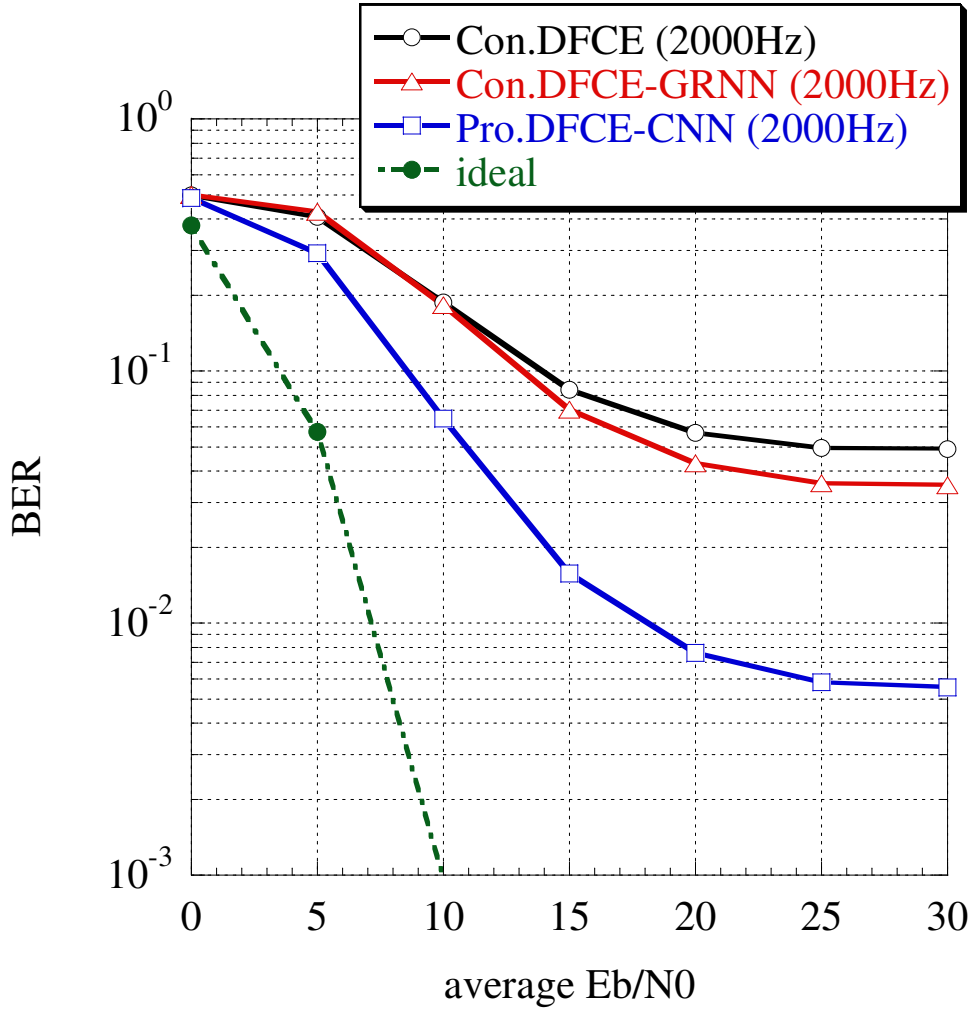


Figure 2.10: BER performance compared to various conventional methods at max Doppler frequency of 2000Hz.

respectively. In the case of maximum Doppler of 1000 Hz, only DFCE and conventional GRNN have an error floor at 10^{-4} . The proposed method moves the error floor and achieves the reasonable BER performance below 10^{-5} , which is the closest to the actual channel. Furthermore, compared to conventional methods, there is a

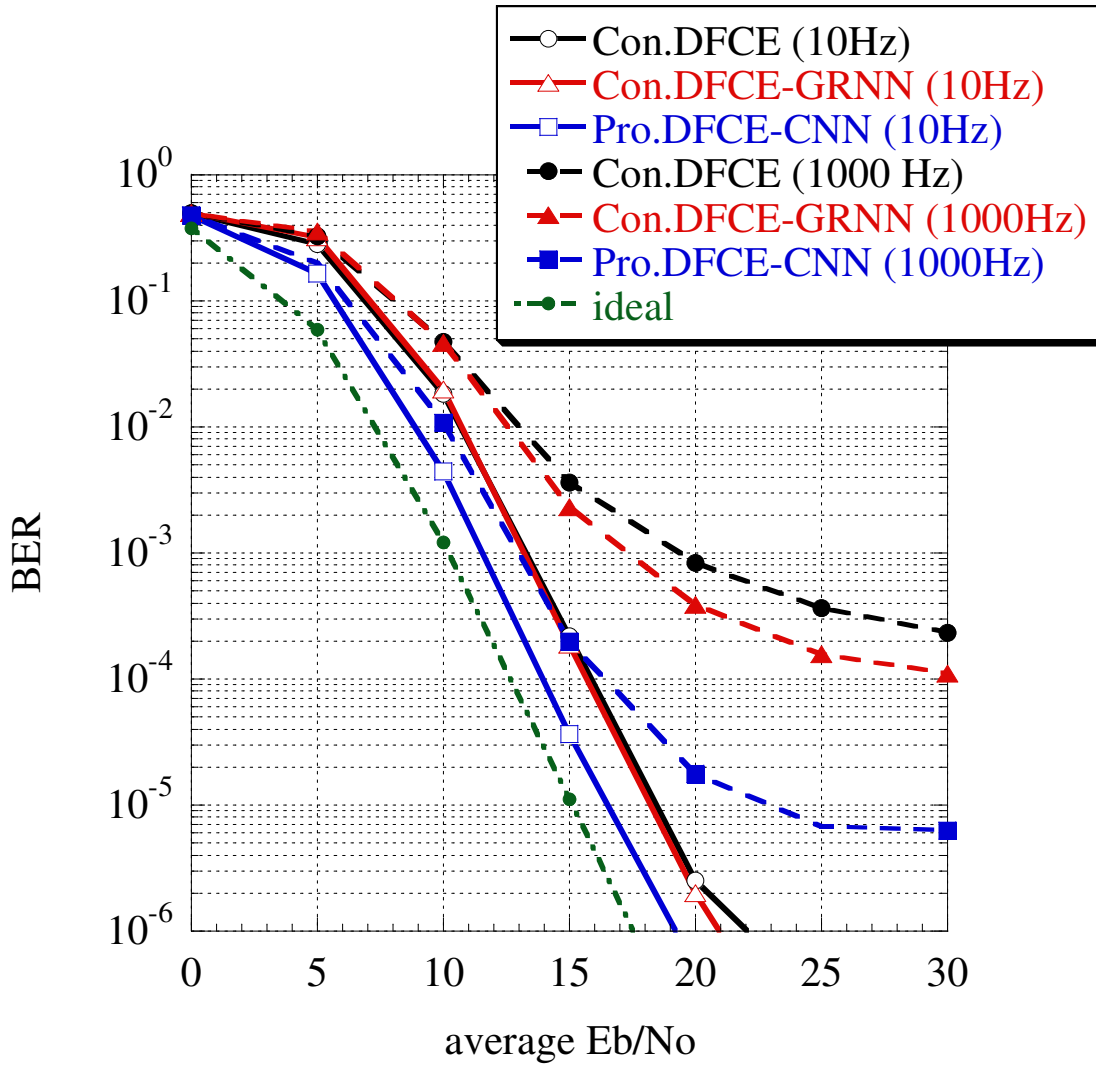


Figure 2.11: BER performance compared to various conventional methods at lower Doppler frequency.

significant BER improvement in the environment with a small Doppler frequency shift of 10 Hz, whether the system is in low or high SNR. This is because when the Doppler frequency shift becomes lower, the channel image of DFCE has fewer time-varying characteristics arising from Doppler shifts, and the CNN also provides

highly accurate estimated CSIs based on these simpler characteristics.

Therefore, regression CNN greatly enhances channel tracking performances in a high-mobility environment. As seen from the above result, the DFCE-aided CNN method is extremely effective even in various high Doppler frequency shift scenarios and outperforms the conventional methods.

Table 2.3: Time cost by various methods.

	Processing time [ms]	BER
GRNN	0.055858	3.5×10^{-2}
Proposal	0.008317	1.8×10^{-3}

We compare the GRNN and regression CNN methods by the CPU processing time consumed for BER performance at SNR=30 dB and the maximum Doppler frequency of 2000 Hz, as summarized in Table 2.3. As can be seen from the table, the CNN is faster than the GRNN in terms of processing speed. This is because CNNs perform offline learning beforehand, unlike the GRNN method. In the meantime, the BER performance of the proposed method can be considerably improved; it could be applicable for practical hardware implementation due to the feasible execution time.

Although higher tracking performance can be achieved by using a two-dimensional scattered pilot, the proposed method can achieve high tracking performance even with only a pilot symbol set at the beginning of the packet by applying machine learning. The proposed method can achieve high transmission efficiency since it can reduce the overhead caused by the pilot structure. The proposed method can also be applied under the scattered pilot arrangement, which would provide a further equalization performance improvement. It should be investigated in our future

work.

2.7 Conclusion

In this paper, a regression CNN-based channel estimation method utilizing the image of the initially estimated channel has been proposed to compensate for rapidly changing channels. The initially estimated channel consisting of a two-dimensional time and frequency domain response is obtained by DFCE. The two-dimensional extracted features using CNN can significantly improve the overall channel tracking capability of the system by reducing the impact of errors in the DFCE arising from the selective fading in the time and frequency domain. Thus, even at a maximum Doppler frequency of 2000 Hz, the proposed method can outperform the previous GRNN-based method in terms of BER performance. In addition, it is shown that the BER performance can also be improved for different SNR and Doppler frequencies without any estimator due to the generalization of the CNN, indicating that the proposed method is universal in a variety of situations.

Bibliography

- [1] F. A. Dietrich and W. Utschick, “Pilot-assisted channel estimation based on second-order statistics,” *IEEE Transactions on Signal Processing*, Vol. 53, No. 3, pp. 1178-1193, Mar.2005.
- [2] M. Yofune, C. Ahn, T. Kamio, H. Fujisaka, and K. Haeiwa, “Decision direct and linear prediction based fast fading compensation for TFIOFDM,” *Far East J. Electron. Commun.*, Vol. 3, No. 1, pp. 35-52, Jul. 2007.
- [3] F. Adachi, “BER analysis of 2PSK, 4PSK, and 16QAM with decision feedback channel estimation in frequency-selective slow Rayleigh fading, ’’ *IEEE Trans. Veh. Technol.*, vol. 48, no. 5, pp. 1563–1572, Sep. 1999.
- [4] D. Li, S. Feng and W. Ye, “Pilot-assisted channel estimation method for OFDMA systems over time-varying channels,” *IEEE communications letters*, Vol. 13, No. 11, pp. 826-828, Jun. 2009.
- [5] Z. Tang and G. Leus, “Pilot schemes for time-varying channel estimation in OFDM systems,” *2007 IEEE 8th Workshop on Signal Processing Advances in Wireless Communications*, pp. 1-5, 2007.
- [6] H. Ye, G. Y. Li and B. -H. Juang, “Power of Deep Learning for Channel Estimation and Signal Detection in OFDM Systems,” *IEEE Wireless Communications Letters*, Vol. 7, No. 1, pp. 114-117, Feb. 2018.

- [7] Y. Liao, Y. Hua and Y. Cai, “deep Learning Based Channel Estimation Algorithm for Fast Time-Varying MIMO-OFDM Systems,” *IEEE Communications Letters*, Vol. 24, No. 3, pp. 572-576, Mar. 2020.
- [8] T. Omura, S. Kojima, K. Maruta, and C.-J. Ahn, “Neural network based channel identification and compensation,” *IEICE Commun. Exp.*, Vol. 8, No. 10, pp. 416-421, 2019.
- [9] T. Omura, N. Hoyer, K. Maruta, and C.-J. Ahn, “Improving ANN based channel identification and compensation using GRNN method under fast fading environment,” *2019 International Conference on Advanced Technologies for Communications (ATC)*, pp. 28-32, Oct. 2019.
- [10] Y. Asai, J. Mashino, T. Sugiyama, M. Katayama, “A simple channel tracking scheme using deductive combining for MIMO-OFDM WLANs”, *IEICE Communications Express*, vol. 6, no. 7, p. 429-434, Jul. 2017.
- [11] T. L. Singal, “Wireless communications,” Tata McGraw-Hill Education, 2010.
- [12] J. Proakis, “Digital Communications,” McGraw-Hill, Nov. 2007.
- [13] S. Soejima, Y. Ida, C.-J. Ahn, T. Omori, and K.-Y. Hashimoto, “Fast fading compensation based on weighted channel variance for TFI-OFDM,” *J. Signal Process.*, Vol. 17, No. 3, pp. 41-49, 2013.
- [14] T. Omura, N. Hoyer, K. Maruta, and C. Ahn, “Improving ANN based Channel Identification and Compensation using GRNN Method under Fast Fading Environment,” *Proc. The 2019 International Conference on Advanced Technologies for Communications (ATC)*, pp. 28-32, October 2019.
- [15] D. Specht, “A general regression neural network,” *IEEE Transactions on Neural Networks*, vol. 2, no. 6, pp. 568-576, November 1991.

- [16] M. Raheema, and A. Abdullah, “Function Approximation using Neural and Fuzzy Methods,” *Communications on Applied Electronics*, vol. 6, no. 3, pp. 35-42, November 2016.
- [17] S. Yang, T. Ting, K. Man, and S. Guan, “Investigation of Neural Networks for Function Approximation,” *Procedia Computer Science*, vol. 17, pp. 586-594, December 2013.
- [18] F. Heimes and B. Heuvein, “The normalized radial basis function neural network,” *Proc. IEEE Int. Conf. Syst., Man, Cybern.*, vol. 2, pp. 1609–1614, Nov. 2013.
- [19] M. Soltani, V. Pourahmadi, A. Mirzaei and H. Sheikhzadeh, “Deep learning-based channel estimation.” *IEEE Communications Letters*, Vol. 23, No. 4, pp. 652-655, 2019.
- [20] S. Kojima, K. Maruta, Y. Feng, C. Ahn, and V. Tarokh, “CNN based Joint SNR and Doppler Shift Classification using Spectrogram Images for Adaptive Modulation and Coding,” *IEEE Transactions on Communications*, Vol. 69, No. 8, pp. 5152-5167, Aug. 2021
- [21] B. Zhang et al., “A 5G Trial of Polar Code,” *IEEE Globecom Workshops (GC 2016 Wkshps)*, pp. 1-6, Dec. 2016.

Chapter 3

Data-aided weight with subcarrier grouping for Adaptive Array Interference Suppression

3.1 Introduction

With the advent of Internet-of-Things (IoT), mobile data traffic, as well as the number of movable devices and connections, has been rapidly increasing in cellular networks. Increasing transmission rates and realizing huge system capacity are essential for the fifth generation of mobile communications (5G) and beyond [1],[2]. Therefore, millimeter wave (mmWave) is used as the ideal communication technology to solve the above problems [3]. Millimeter wave communication systems exploit the ultra-high frequency (EHF) band for broadband communications where there is still a large amount of available spectrum for communications [4]. However, it suffers from severe propagation loss, causing restricted coverage and a link budget shortfall. The deployment of a massive MIMO-small cell system [5] is one of the promising solutions to reduce the attenuation of radio waves. By setting the phase shifts of

all the antenna elements to obtain beamforming gain, the signal-to-interference plus noise ratio (SINR) can be maximized in massive MIMO. Small cells can manage high traffic demand within the coverage area of macrocells [6],[7]. In the small cells, the propagation environment is dominated by a line of sight (LOS) component for a reliable communication system. Therefore, Rician distribution with LOS and non-LOS (NLOS) components is considered as the channel model in this situation [8].

In general, inter-user-interference (IUI) and additive white Gaussian noise are essential for array antenna. Sample matrix inversion(SMI) [9],[10] is a well-known method for interference suppression adaptive array antennas. SMI utilizes a covariance matrix derived from the pilot symbols and the received signals of each antenna element to calculate desirable weights. Due to the inaccurate channel state information (CSI) caused by the additive noise effect, this method requires a sufficient number of samples to adequately suppress interference [11]. In addition, since the array weights are calculated for each subcarrier in orthogonal frequency division multiplexing (OFDM) systems, it causes not only an insufficient number of samples but also a large amount of computation [12]. Further discussion is needed for the OFDM frame. Common Correlation Matrix (CCM) based SMI algorithm has been proposed to reduce the amount of calculation and enhance weight precision for interference suppression performance. In the CCM method, an adequate number of the time domain signal samples can be available for a well-converged covariance matrix [13], [14]. However, it still has a problem of inaccurate channel estimation and the limitation of working only in an almost frequency-flat fading environment since the weight is common in all subcarriers. For this reason, it cannot work in the heterogeneous deployment of small cells. A more recent work evaluates the effect under the above situation [15]. Reference [15] proposed an adaptive sub-carrier grouping (ASG) method. In ASG method, the standard deviations among the adjacent subcarriers are calculated, averaged, and compared with the threshold

to determine the grouping. It has good performance even in frequency selectivity channels. However, because of an insufficient number of signal samples under the limited number of pilot symbols, there is a problem of insufficient noise suppression performance and the threshold of the grouping must depend on signal-to-noise ratio (SNR). Although there are many methods to estimate SNR [16]-[18], they not only cause the additional computational complexity but the SNR estimation errors, which must be considered in the ASG method.

This paper proposes to introduce data-aided weight calculation with subcarrier grouping. The proposed method calculates weights by the SMI method with subcarrier grouping and determines the decision result. The benefit of our proposal is that we do not need to know the SNR or other information. This is because the number of subcarriers in each group is the same. In general, more pilot symbols have been used to improve the accuracy of weights. However, an increased number of pilot symbols causes poor transmission efficiency since they do not contribute to data transfer. Another key feature of our proposed method is to expand toward the symbol direction by increasing the amount of sample aided by decision feedback data, which can not only estimate more accurate weight estimation but also maintain transmission efficiency. Moreover, the LMS algorithm with low computational complexity is introduced to ensure convergence while using the initial weights to avoid additional iterations.

The rest of this paper is organized as follows. The system model is defined and conventional schemes are introduced in Section 3.2. Section 3.3 describes the proposed scheme. Computer simulation results are presented in Section 3.4. Finally, Section 3.5 concludes this paper.

3.2 System model

3.2.1 Channel model

In the Rician fading channel model, there are two components: a deterministic component corresponding to LOS signals and a random component corresponding to NLOS signals [20]. An NLOS multipath fading channel is expressed as,

$$h(\tau)_{\text{NLOS}} = \sum_{l=1}^L h_l \delta(t - \tau_l), \quad (3.1)$$

where δ denotes the Dirac's delta function, τ_l is the time delay of the l -th path and L is the total number of paths. h_l indicates the complex channel coefficient, which is represented as follows known as Jakes' model [21],

$$h_l = \frac{g_l}{\sqrt{J}} \sum_{j=1}^J \exp(j\phi_j), \quad (3.2)$$

where g_l denotes the gain of the path. J rays arrive at the receiver with an initial phase ϕ_j . Here assumes the normalized path gain, i.e. $\sum_{l=0}^L E[|h_l^2|] = 1$ where $E[\cdot]$ stands for the ensemble average operation. The Rician fading channel is expressed as,

$$h(\tau) = \left[\frac{K}{K+1} \right]^{\frac{1}{2}} h_{\text{LOS}}(\tau) + \frac{h_{\text{NLOS}}(\tau)}{(K+1)^{\frac{1}{2}}}, \quad (3.3)$$

$$h_{\text{LOS}}(\tau) = h_0 \delta(t - \tau_1), \quad (3.4)$$

$$h_0 = g_0 \exp(j\phi_0), \quad (3.5)$$

where $h_{\text{LOS}}(\tau)$ represents the LOS fading channel and h_0 is the complex channel coefficient, respectively. Then the frequency response $H(f)$ is obtained by Fourier transform of the impulse response as,

$$H(f) = \sum_{l=0}^{N_{\text{FFT}}-1} h(\tau_l) \exp\left(-j \frac{2\pi f \tau_l}{N_{\text{FFT}}}\right), \quad (3.6)$$

where f and N_{FFT} denote the frequency component and the number of fast Fourier transform (FFT) points, respectively.

3.2.2 Uplink Array Antenna System Model

We suppose uplink transmission where a base station (BS) has N_r elements array antenna and N_u user terminals (UEs) with OFDM like Fig.3.1.

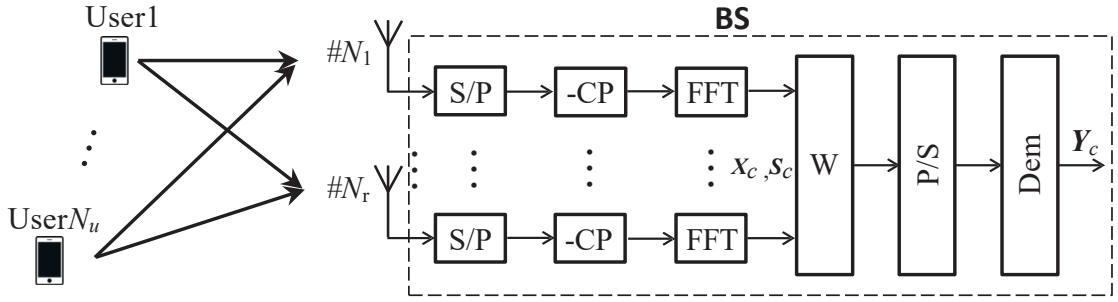


Figure 3.1: Block diagram of the basic system.

Throughout this paper, subscripts c and u represent the c -th subcarrier and the u -th user, respectively. Then, the received pilot signal $\mathbf{X}_c \in \mathbb{C}^{N_r \times N_p}$, received data signal $\mathbf{S}_c \in \mathbb{C}^{N_r \times N_d}$, and array output $\mathbf{Y}_c \in \mathbb{C}^{N_u \times N_d}$ can be expressed as follows.

$$\mathbf{X}_c = \mathbf{A}\mathbf{H}_c\mathbf{P}_c + \mathbf{N}, \quad (3.7)$$

$$\mathbf{S}_c = \mathbf{A}\mathbf{H}_c\mathbf{D}_c + \mathbf{Z}, \quad (3.8)$$

$$\mathbf{Y}_c = \mathbf{W}_c^H \mathbf{S}_c, \quad (3.9)$$

where

$$\mathbf{A} = [\mathbf{a}_1, \dots, \mathbf{a}_u, \dots, \mathbf{a}_{N_u}], \quad (3.10)$$

$$\mathbf{H}_c = \text{diag}(H_1, \dots, H_u, \dots, H_{N_u}), \quad (3.11)$$

$$\mathbf{P}_c = [\mathbf{p}_1^T, \dots, \mathbf{p}_u^T, \dots, \mathbf{p}_{N_u}^T]^T, \quad (3.12)$$

$$\mathbf{D}_c = [\mathbf{d}_1^T, \dots, \mathbf{d}_u^T, \dots, \mathbf{d}_{N_u}^T]^T. \quad (3.13)$$

$\mathbf{A} \in \mathbb{C}^{N_r \times N_u}$, $\mathbf{H}_c \in \mathbb{C}^{N_u \times N_u}$, $\mathbf{P}_c \in \mathbb{C}^{N_u \times N_p}$, $\mathbf{D}_c \in \mathbb{C}^{N_u \times N_d}$, $\mathbf{N} \in \mathbb{C}^{N_r \times N_p}$, $\mathbf{Z} \in \mathbb{C}^{N_r \times N_d}$, $\mathbf{W}_c \in \mathbb{C}^{N_r \times N_u}$ denote array factor matrix, fading channel matrix, transmitted pilot symbols, transmitted data symbol, additive white Gaussian noise (AWGN) matrices of pilot symbols and data symbols, and weight vector, respectively. The array weight vector can cancel interference components.

3.2.3 SMI Algorithm

SMI algorithm is based on a minimum mean square error (MMSE) method for solving the minimum searching problem [9], whose weight can be derived as,

$$E[|e|^2] = E[|\mathbf{P}_c - \mathbf{W}_c^H \mathbf{X}_c|^2]. \quad (3.14)$$

where the pilot symbol \mathbf{P}_c is considered as the desired response.

The optimal weight by SMI algorithm is derived as

$$\mathbf{\Phi}_c = \mathbf{X}_c \mathbf{X}_c^H, \quad (3.15)$$

$$\mathbf{V}_c = \mathbf{X}_c \mathbf{P}_c^H, \quad (3.16)$$

$$\mathbf{W}_c = \mathbf{\Phi}_c^{-1} \mathbf{V}_c, \quad (3.17)$$

where $\mathbf{\Phi}_c \in \mathbb{C}^{N_r \times N_r}$ and $\mathbf{V}_c \in \mathbb{C}^{N_r \times N_u}$ indicate the covariance matrix and the estimated CSI vector, respectively. However, there is a noise problem in the received signal.

3.2.4 Adaptive Subcarrier Grouping (ASG)

In the above scheme, the effect of noise has been not fully considered when calculating the array weight. By exploiting adaptive grouped subcarriers with correlated frequency responses for averaging, the convergence precision of the covariance matrix can be improved [15]. First, subcarriers are chosen for grouping to suppress

interference. We define m as both the number of stages and the end sequence of a group to delimit a group range from the c -th subcarrier, i.e., the subcarrier sequence corresponding to a group in the m -th stage is $(c, \dots, c + m)$. $m = 0$ is initialized as no grouping.

We average the grouped received signal X and pilot signal P from subcarrier c to $c+m$ to reduce noise, which combines the $(m+1)$ subcarriers. The grouped received pilot signal matrix and the grouped transmitted pilot signal matrix for averaging is calculated as follows,

$$\overline{\mathbf{X}}^{(m)} = \frac{1}{m+1} \sum_{k=0}^m \mathbf{X}_{c+k}, \quad (3.18)$$

$$\overline{\mathbf{P}}^{(m)} = \frac{1}{m+1} \sum_{k=0}^m \mathbf{P}_{c+k}, \quad (3.19)$$

where $X_{c+k} \in \mathbb{C}^{N_r \times N_p}$ and $P_{c+k} \in \mathbb{C}^{N_u \times N_p}$ are the $(c+k)$ -th subcarrier of the received pilot signal matrix and transmitted pilot signal matrix. $\overline{\mathbf{X}}^{(m)} \in \mathbb{C}^{N_r \times N_p}$ and $\overline{\mathbf{P}}^{(m)} \in \mathbb{C}^{N_u \times N_p}$ are the averaged received pilot signal and averaged transmitted pilot signal. Then, a standard deviation of the grouped received signal, $\sigma_{\text{ASG}}^{(m)} \in \mathbb{C}^{N_r \times N_p}$ is calculated as,

$$\sigma_{\text{ASG}}^{(m)} = \sqrt{\frac{1}{m+1} \sum_{k=0}^m \left\{ \mathbf{X}_{c+k} - \overline{\mathbf{X}}^{(m)} \right\}^2}, \quad (3.20)$$

$$\overline{\sigma_{\text{ASG}}^{(m)}} = \sum_{j=1}^{N_p} \sum_{i=1}^{N_r} \sigma_{\text{ASG},i,j}^{(m)} / N_p N_r. \quad (3.21)$$

$\overline{\sigma_{\text{ASG}}^{(m)}}$ represents the dispersion among the grouped subcarriers. Therefore, only frequency-correlated subcarriers are combined by comparing with a threshold value, $\sigma_{\text{ASG}}^{\text{th}}$, as follows.

if $\overline{\sigma_{\text{ASG}}^{(m)}} < \sigma_{\text{ASG}}^{\text{th}}$, grouping operation proceeds to the next stage;

$$m \leftarrow m + 1. \quad (3.22)$$

Otherwise, if $\overline{\sigma_{\text{ASG}}^{(m)}} > \sigma_{\text{ASG}}^{\text{th}}$, the grouping process is terminated, and the array weight is calculated;

$$\hat{\mathbf{X}}_{c+k} = \overline{\mathbf{X}^{(m)}}, \quad (3.23)$$

$$\hat{\mathbf{P}}_{c+k} = \overline{\mathbf{P}^{(m)}}, \quad (3.24)$$

$$\Phi_{\text{SG}}^{c+k} = \hat{\mathbf{X}}_{c+k} \hat{\mathbf{X}}_{c+k}^{\text{H}}, \quad (3.25)$$

$$\hat{\mathbf{V}}_{c+k} = \hat{\mathbf{X}}_{c+k} \hat{\mathbf{P}}_{c+k}^{\text{H}}, \quad (3.26)$$

$$\hat{\mathbf{W}}_{c+k} = (\Phi_{\text{SG}}^{c+k})^{-1} \hat{\mathbf{V}}_{c+k}, \quad (3.27)$$

where $\hat{\mathbf{X}}_{c+k} \in \mathbb{C}^{N_r \times N_p}$, $\hat{\mathbf{P}}_{c+k} \in \mathbb{C}^{N_u \times N_p}$, $\Phi_{\text{SG}}^{c+k} \in \mathbb{C}^{N_r \times N_r}$, $\hat{\mathbf{V}}_{c+k} \in \mathbb{C}^{N_r \times N_u}$, $\hat{\mathbf{W}}_{c+k} \in \mathbb{C}^{N_r \times N_u}$ denote the averaged received signal for grouping, the pilot signal matrix for grouping, the covariance matrix, CSI, and the proposed weight matrix at the $(c+k)$ -th subcarrier ($k = 0, \dots, m$), respectively. Therefore, the optimal group size can be obtained. If $\sigma_{\text{ASG}}^{\text{th}}$ is set to an appropriate value, the ability to mitigate noise can be enhanced, contributing to better weight derivation.

3.3 Proposal: Subcarrier grouping with data-aided weight

In the adaptive subcarrier grouping, since setting a threshold too large degrades weight derivation accuracy due to an excess of data symbols having uncorrelated frequency characteristics, setting the appropriate value of $\sigma_{\text{ASG}}^{\text{th}}$ holds a prominent factor. SNR is considered to be the main factor involved in setting the threshold. Therefore, SNR estimation needs to be applied, such as some comparisons and novel algorithms [16]-[17]. However, if these algorithms are applied, it will increase the complexity of communication. [15] does not consider the computational problem and estimation accuracy. In the proposed method, we not only reduce the noise effect by increasing the number of data-aided samplings but also reduce the computational

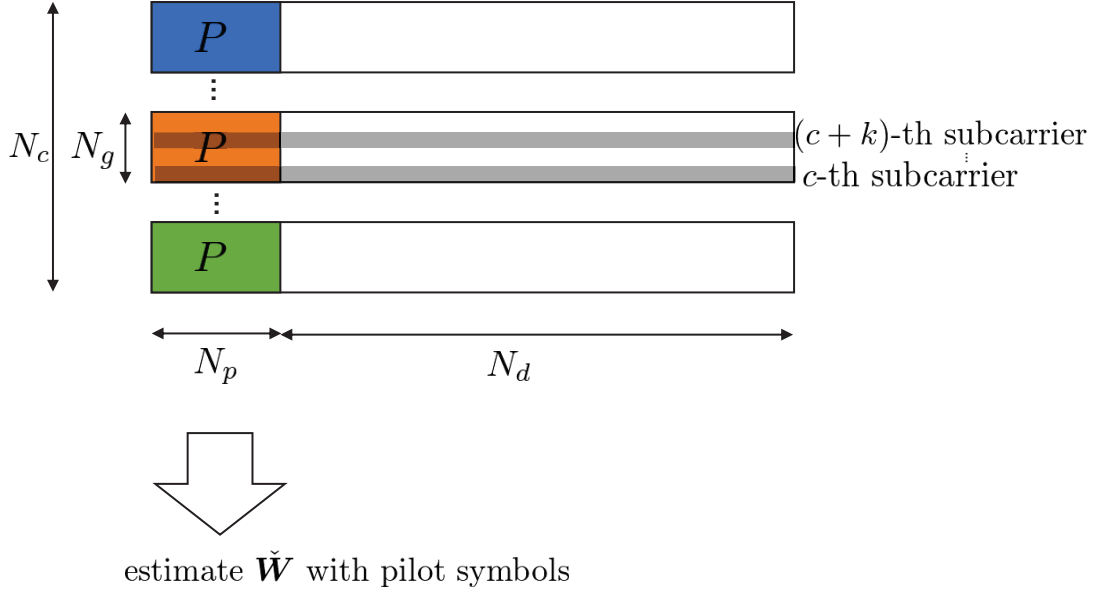


Figure 3.2: Initial weight $\check{\mathbf{W}}$ calculation with subcarrier grouping.

complexity while ensuring transmission efficiency. At this time, we do not use the additional pilot symbols. Our method is divided into two steps: 1. Deriving decision result of array output by the SMI with subcarrier grouping, 2. Obtaining a more accurate CSI vector aided by feedback decision data and estimating weight by LMS scheme with subcarrier grouping.

3.3.1 Initial Weight Calculation

Initial weight is calculated by SMI weight, which uses subcarrier grouping. Different from ASG, the grouping is not established according to the threshold. Each group is directly composed of the same number of subcarriers and the number of subcarriers is N_g . The initial weight $\check{\mathbf{W}}_{c+k}$ ($k = 0, \dots, N_g - 1$) is calculated from (3.23) to (3.27). The range of the group from the c -th subcarrier is directly delimited as

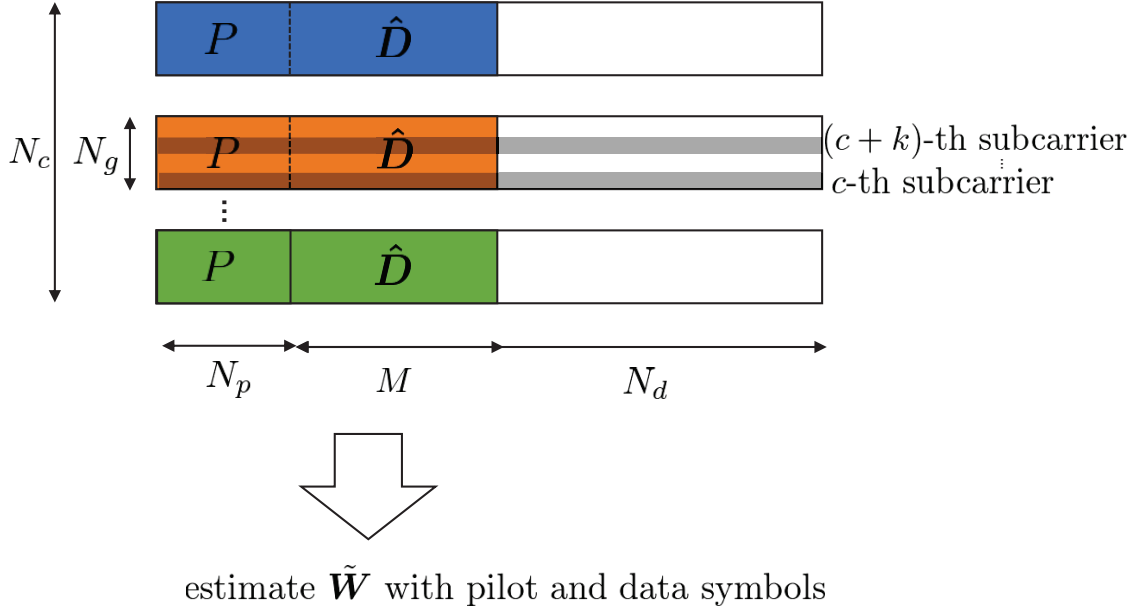


Figure 3.3: Proposed weight $\tilde{\mathbf{W}}$ calculation with subcarrier grouping.

follows, without iteration,

$$m + 1 = N_g. \quad (3.28)$$

The array output for the c -th subcarrier is written by,

$$\mathbf{Y}_c = \tilde{\mathbf{W}}_c^H \mathbf{S}_c. \quad (3.29)$$

Due to the noise effect, the initial array output contains errors. It is mapped into the original QAM constellation points and the initial solution $\hat{\mathbf{D}}_c$ is obtained as follows,

$$\hat{\mathbf{D}}_c = \mathcal{F}(\mathbf{Y}_c), \quad (3.30)$$

where $\mathcal{F}(\cdot)$ represents the decision function. In order to reduce the amount of calculation, $\hat{\mathbf{D}}_c$ is only determined by the M ($0 \leq M \leq N_d$) symbols instead of all. The concept of initial weight estimation for the SMI with subcarrier grouping

is shown in Fig. 3.2. Each group corresponding to a different color contains N_g subcarriers.

3.3.2 Data-aided Weight Calculation

In the data-aided weight calculation scheme, the subcarrier grouping is also used and $\hat{\mathbf{D}}_c$ can be regarded as an additional pilot signal for weight calculation and combined with the pilot signal as follows,

$$\tilde{\mathbf{D}}_c = [\mathbf{P}_c, \hat{\mathbf{D}}_c], \quad (3.31)$$

where $\tilde{\mathbf{D}}_c$ is desired response. The desired response in the subcarrier grouping can be derived as,

$$\bar{\mathbf{D}} = \frac{1}{N_g} \sum_{k=0}^{N_g-1} \tilde{\mathbf{D}}_{c+k}. \quad (3.32)$$

where the number of subcarrier grouping for the desired responses is N_g , similar to (3.19) and (3.28). Because of the inverse matrix operation, the repeated use of the SMI method results in a significant increase in computation. Therefore, we use the initial weight $\tilde{\mathbf{W}}_c$ and the LMS method to replace SMI.

$$\tilde{\mathbf{W}}_{c+k}(1) = \tilde{\mathbf{W}}_{c+k}, \quad (3.33)$$

$$\begin{aligned} \tilde{\mathbf{W}}_{c+k}(n+1) &= \tilde{\mathbf{W}}_{c+k}(n) \\ &+ \beta \tilde{\mathbf{X}}_{c+k} (\bar{\mathbf{D}}^H - \tilde{\mathbf{X}}_{c+k}^H \tilde{\mathbf{W}}_{c+k}(n)), \end{aligned} \quad (3.34)$$

where n and β denote the number of iterations and the step size that can control the convergence characteristics of the LMS algorithm, respectively. $\tilde{\mathbf{W}}_{c+k}(n) \in \mathbb{C}^{N_r \times N_u}$ represents the weight at the $(c+k)$ -th subcarrier in the n -th step of the LMS algorithm ($k = 0, \dots, N_g-1$). $\tilde{\mathbf{X}}_{c+k} \in \mathbb{C}^{N_r \times (N_p+M)}$ indicates the signal containing the X_c and the first M data symbols of the S_c with grouping and averaging. Grouping and averaging are performed as (3.23). In addition, since the initial state of the weight

Algorithm 1 Proposed interference suppression scheme

- 1: $\tilde{\mathbf{W}}_{c+k} \leftarrow (\Phi_{\text{SG}}^{c+k})^{-1} \hat{\mathbf{V}}_{c+k}$
 - 2: $\mathbf{Y}_c \leftarrow \tilde{\mathbf{W}}_c^H \mathbf{S}_c$
 - 3: $\hat{\mathbf{D}}_c \leftarrow \mathcal{F}(\mathbf{Y}_c)$
 - 4: $\tilde{\mathbf{D}}_c = [\mathbf{P}_c, \hat{\mathbf{D}}_c]$
 - 5: $\bar{\mathbf{D}} \leftarrow \frac{1}{N_g} \sum_{k=0}^{N_g-1} \tilde{\mathbf{D}}_{c+k}$
 - 6: $n \leftarrow 1$
 - 7: $\tilde{\mathbf{W}}_{c+k}(n) \leftarrow \tilde{\mathbf{W}}_{c+k}$
 - 8: **while** $n > L$ **do**
 - 9: $\tilde{\mathbf{W}}_{c+k}(n+1) \leftarrow \text{lms}[\tilde{\mathbf{W}}_{c+k}(n), \bar{\mathbf{D}}]$
 - 10: $n \leftarrow n + 1$
 - 11: **end while**
 - 12: *lms[.] denotes the least mean square function
-

is calculated by the SMI algorithm, the number of iterations required for convergence can be decreased. Consequently, the amount of computation is reduced. It is worth noting that since the convergence rate of LMS without the initial weight is slower than SMI[22][23], a large number of iterations must be performed to achieve the same satisfactory convergence as SMI. In other words, LMS without the initial weight is more computationally intensive than SMI in order to achieve the same effect. That is why the LMS cannot be used in the initial weight calculation. By repeating the above procedures, the weight error can be minimized. The concept of data-aided weight derivation for the LMS with subcarrier grouping is shown in Fig. 3.3. Algorithm 1 summarizes the detailed procedure (3.28)-(3.34).

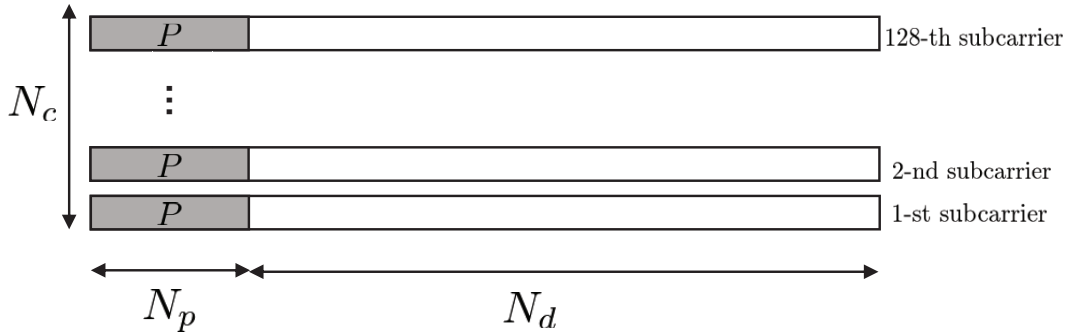


Figure 3.4: Frame structure.

3.4 Computer Simulation

3.4.1 Simulation Parameters

We examine the interference suppression performance of the proposed algorithm by a computer simulation. Detailed simulation parameters are listed in Table 3.1. The receiver using $N_r = 16$ rectangular array antenna elements attempts to separate out one desired signal from $N_u = 4$ incoming signals. We employ 16QAM modulation to every frame consisting of $N_p = 4$ pilot and $N_d = 30$ data symbols, and each frame is shown in Fig. 3.4. Moreover, each OFDM symbol is composed of $N_c = 128$ subcarriers. Rician fading with multipath is considered. The bandwidth of the transmission signal is 1.25 MHz, and the OFDM symbol duration is $T_s = 71.4 \mu\text{s}$, then the OFDM symbol rate is about $1/T_s = 14$ kHz. These parameters are almost compatible with a compact cellular system, i.e. LTE system [24].

3.4.2 Simulation Results

Figs. 3.5 and 3.6 show the BER performance comparison between the conventional SMI, CCM-SMI, adaptive subcarrier grouping [15], and the proposed method. The effect of the conventional and proposed methods is evaluated with different LOS

Table 3.1: Simulation parameters

Parameters	Values
Number of receiver antennas N_r	16
Number of signal sources N_u	4
Transmission scheme	OFDM
Subcarrier spacing	15 kHz
Symbol duration T_s	71.4 μ s
Modulation order	16QAM (w/o FEC)
Number of pilot symbols N_p	4
Number of data symbols N_d	30
Number of subcarriers N_c	128
Number of FFT points N_{FFT}	128
Angle of desired signal	0°
Angles of interference signals	30°, -70°, 80°
Channel model	Rician fading
Rician K factor	10,-10 dB
Max Doppler frequency f_d	10 Hz ($f_d T_s = 4.0 \times 10^{-5}$)

components. Rician K factors, i.e. $K = 10, -10$ dB, present whether the LOS component dominates the channel. When $K = -10$ dB, it approximates Rayleigh fading with no dominant LOS path. In the adaptive subcarrier grouping method, the value

of σ_{ASG} according to the SNR and shown as follows,

$$\sigma_{\text{ASG}} = \sqrt{\frac{10^{-3/10}}{\text{SNR}}}, \quad (3.35)$$

To achieve convergence while reducing the computational complexity, we set $M = 15$, $\beta = 0.6$, $L = 2$, $N_g = 4$ in the proposed method.

The proposed method has better BER performance than other conventional methods at arbitrary K factors. In a large $K = 10$ dB factor, the achievable gain is around 1.5 dB compared to ASG, and 4 dB compared to MMSE-SMI at 10^{-4} BER. Furthermore, in a smaller $K = -10$ dB situation, the proposed method also shows the best BER performance, where the achievable gain is around 1 dB compared to MMSE-SMI. However, although CCM-SMI can suppress the noise effect, the BER performance seriously deteriorates and the error floor is observed before 10^{-4} or 10^{-2} because of frequency selectivity. Therefore, it can only be used in a single-path situation. In addition, it is worth noting that ASG needs know the SNR situation to determine the threshold σ_{ASG} and make groups for noise rejection. In Figs. 3.5 and 3.6, the SNR estimation of ASG is assumed to be absolutely correct without considering the accuracy. If the performance of the SNR estimation method deteriorates, ASG will become ineffective. In addition, the proposed method does not depend on the SNR. It uses the same number of subcarrier groupings and decision feedback to improve BER performance.

3.4.3 Computation Complexity

Since a large number of weight calculations require huge memory and hardware resources, it is crucial to minimize the amount of computation with maintaining good performance. The number of complex-valued multiplications is used to evaluate the amount of computation.

Compared with the SMI algorithm, the computation complexity of our proposed

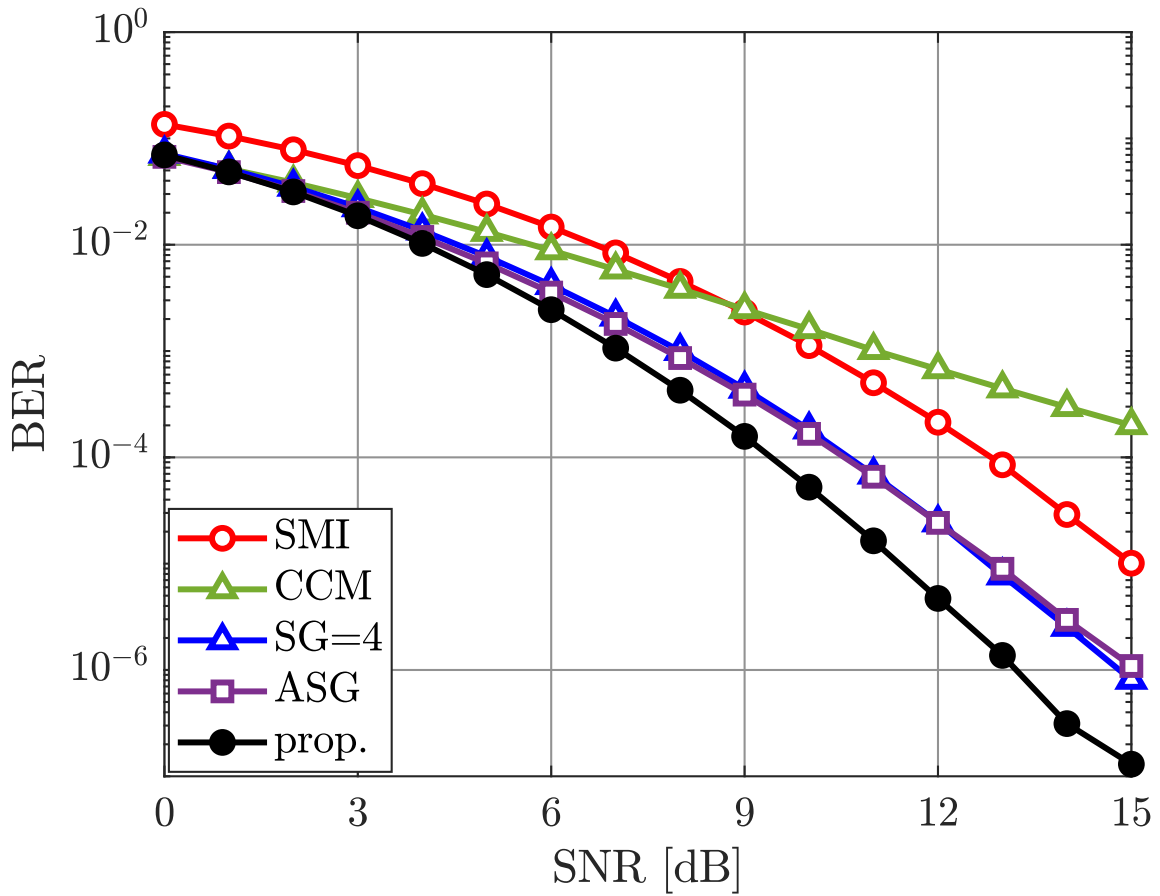


Figure 3.5: BER performance comparison ($K = 10$ dB).

scheme can be reduced by 20.4%. It is worth noting that although the decision feedback causes an increase in the amount of computation, several subcarriers can share one weight in the subcarrier grouping and the LMS algorithm is applied, which reduces the amount of computation. The LMS algorithm reuses the weight from the initial phase as well as replaces matrix inversion that dominates the computational complexity.

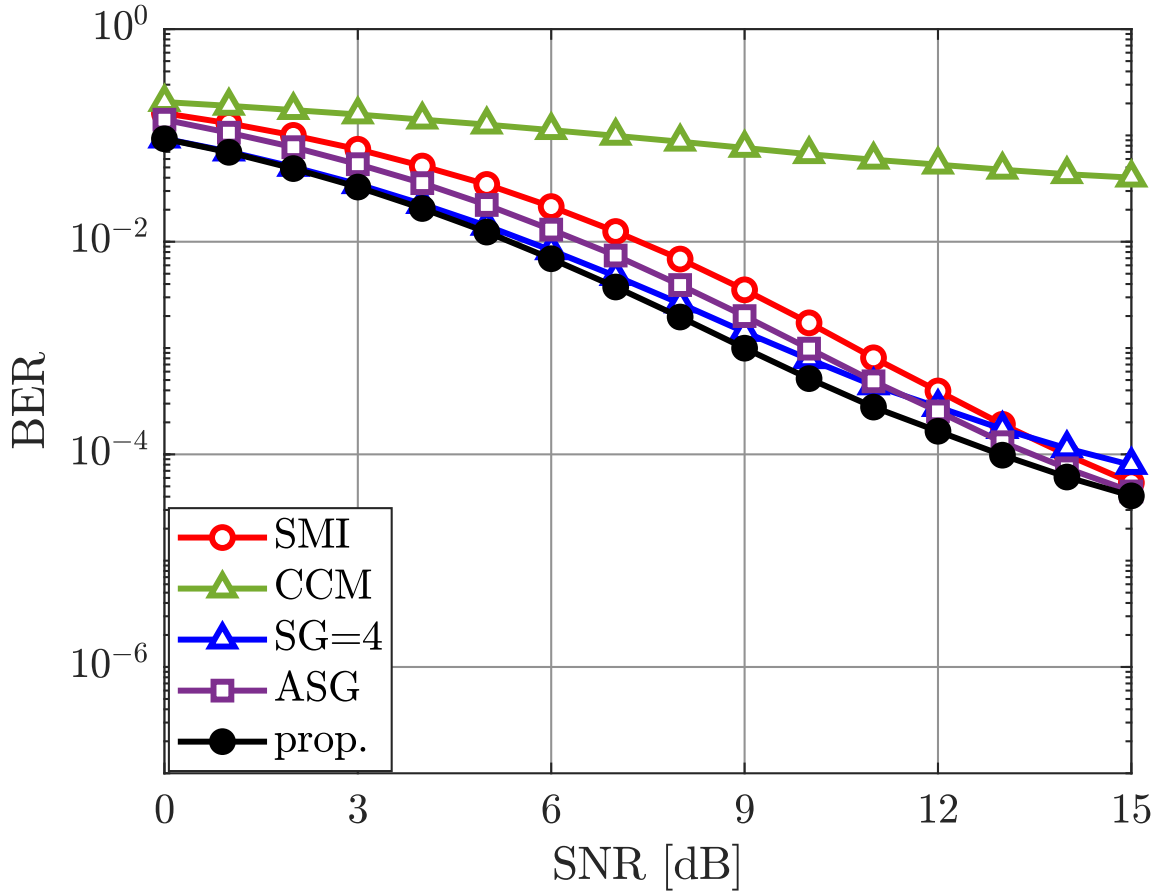


Figure 3.6: BER performance comparison ($K = -10$ dB).

3.5 Conclusion

This paper proposed the data-aided weight calculation and LMS method to improve the interference suppression performance of subcarrier grouping-based SMI adaptive array without SNR estimation method. It focuses on increasing data samples to reduce noise, thus maximizing the array weight derivation precision. Simulation results showed that the proposed method attained improved BER performance significantly with maintaining the transmission efficiency, whether LOS is the major factor or not. In addition, it saves computation compared to the conventional calcu-

Table 3.2: Computation complexity

Algorithms	Values (example values used in simulation)
SMI per subcarrier	$N_r^2 N_p N_c + N_p N_r N_u N_c + N_r^3 N_c + N_r^2 N_u N_c$ (819,200)
Proposed	$(\text{SMI} + 2LN_c N_u (N_p + M) N_r) \frac{1}{N_g} + N_r M N_c N_u +$ $N_c M N_u \log_2(M N_u)$ (651,572)

lation of weight derivation for each subcarrier individually. Therefore, our proposed method can be applied as a potential future interference suppression technique for 5G or beyond, where small cells are heterogeneously deployed on the macro cells.

Bibliography

- [1] X. Chen, D. W. K. Ng, W. Yu, E. G. Larsson, N. Al-Dhahir and R. Schober, “Massive Access for 5G and Beyond,” *IEEE Journal on Selected Areas in Communications*, vol. 39, no. 3, pp. 615-637, Mar. 2021. DOI: 10.1109/JSAC.2020.3019724.
- [2] K. Shafique, B. A. Khawaja, F. Sabir, S. Qazi and M. Mustaqim, “Internet of Things (IoT) for Next-Generation Smart Systems: A Review of Current Challenges, Future Trends and Prospects for Emerging 5G-IoT Scenarios,” *IEEE Access*, vol. 8, pp. 23022-23040, 2020, doi: 10.1109/ACCESS.2020.2970118.
- [3] X. Wang et al., “Millimeter Wave Communication: A Comprehensive Survey,” *IEEE Communications Surveys and Tutorials*, vol. 20, no. 3, pp. 1616-1653, thirdquarter 2018. DOI: 10.1109/COMST.2018.2844322.
- [4] Z. Pi and F. Khan, “An introduction to millimeter-wave mobile broadband systems,” *IEEE Communications Magazine*, vol. 49, no. 6, pp. 101-107, Jun. 2011. DOI: 10.1109/MCOM.2011.5783993.
- [5] E. Björnson, M. Kountouris and M. Debbah, “Massive MIMO and small cells: Improving energy efficiency by optimal soft-cell coordination,” *ICT 2013*, 2013, pp. 1-5. DOI: 10.1109/ICTEL.2013.6632074.

- [6] W. Saad, M. Bennis and M. Chen, “A Vision of 6G Wireless Systems: Applications, Trends, Technologies, and Open Research Problems,” *IEEE Network*, vol. 34, no. 3, pp. 134-142, May/June 2020. DOI: 10.1109/MCOM.2011.5783993.
- [7] T. M. Duong and S. Kwon, “Vertical Handover Analysis for Randomly Deployed Small Cells in Heterogeneous Networks,” *IEEE Transactions on Wireless Communications*, vol. 19, no. 4, pp. 2282-2292, April 2020. DOI: 10.1109/TWC.2019.2963829.
- [8] G. Giunta, C. Hao, and D. Orlando, “Estimation of rician K-factor in the presence of Nakagami-m shadowing for the LOS component,” *IEEE Wireless Commun. Lett.*, vol. 7, no. 4, pp. 550-553, Aug. 2018. DOI: 10.1109/LWC.2018.2794447
- [9] Y. Hara, “Weight-convergence analysis of adaptive antenna arrays based on SMI algorithm,” *IEEE transactions on wireless communications*, vol. 2, no. 4, pp. 749-757, 2003. DOI: 10.1109/TWC.2003.814333
- [10] S. Mubeen, A. M. Prasad and A. J. Rani, “Smart antennas by using LMS and SMI algorithms reduces interference,” *2016 International Conference on Electrical, Electronics, and Optimization Techniques (ICEEOT)*, pp. 204-208, 2016. DOI: 10.1109/ICEEOT.2016.7755027.
- [11] X. Yuan and L. Gan, “Robust adaptive beamforming via a novel subspace method for interference covariance matrix reconstruction,” *Signal Processing*, vol. 130, pp. 233-242, 2017. DOI: 10.1016/j.sigpro.2016.07.008.
- [12] T. Akao, S. Taroda, K. Maruta and C. -J. Ahn, “Improved common correlation matrix based SMI algorithm by channel estimation error minimization with LMS approach,” *2017 20th International Symposium on Wire-*

- less Personal Multimedia Communications (WPMC)*, pp. 63-67, 2017. DOI: 10.1109/WPMC.2017.8301888.
- [13] C. -J. Ahn, and S. Iwao, "Adaptive array antenna based on radial basis function network as multiuser detection for WCDMA," *Electronics Letters*, vol. 38, no. 20, pp. 1208-1210, 2002. DOI: 10.1049/el:20020756.
- [14] K. Shima, K. Maruta and C. -J. Ahn, "Data-aided SMI algorithm using common correlation matrix for adaptive array interference suppression," *IEICE Transactions on Fundamentals of Electronics, Communications and Computer Sciences*, vol. 104, no. 2, pp. 404-411, 2021. DOI: <https://doi.org/10.1587/transfun.2020SDP0001>
- [15] K. Shima, S. Kojima, K. Ito, K. Maruta and C. -J. Ahn, "Adaptive Subcarrier Grouping for MMSE-SMI Adaptive Array Interference Suppression," *IEEE Access*, vol.9, pp. 18361-18372, 2021. DOI: 10.1109/ACCESS.2021.3053989
- [16] S. Kojima, K. Maruta, Y. Feng, C. -J. Ahn and V. Tarokh, "CNN based Joint SNR and Doppler Shift Classification using Spectrogram Images for Adaptive Modulation and Coding," *IEEE Transactions on Communications*, vol. 69, no. 8, pp. 5152-5167, Aug. 2021. DOI: 10.1109/TCOMM.2021.3077565.
- [17] T. Ngo, B. Kelley and P. Rad, "Deep Learning Based Prediction of Signal-to-Noise Ratio (SNR) for LTE and 5G Systems," *2020 8th International Conference on Wireless Networks and Mobile Communications (WINCOM)*, pp. 1-6, 2020. DOI: 10.1109/WINCOM50532.2020.9272470
- [18] J. Tian, T. Zhou, T. Xu, H. Hu and M. Li, "Blind Estimation of Channel Order and SNR for OFDM Systems," *IEEE Access*, vol. 6, pp. 12656-12664, 2018, doi: 10.1109/ACCESS.2017.2788020.

- [19] T. Ngo, B. Kelley and P. Rad, "SNR estimation based on CNN and LSTM in broadcasting channel," *2022 IEEE International Symposium on Broadband Multimedia Systems and Broadcasting (BMSB)*, pp. 1-6, 2022. DOI: 10.1109/BMSB55706.2022.9828573.
- [20] N. Czink, X. Yin, H. OZcelik, M. Herdin, E. Bonek and B. H. Fleury, "Cluster Characteristics in a MIMO Indoor Propagation Environment," *IEEE Transactions on Wireless Communications*, vol. 6, no. 4, pp. 1465-1475, Apr. 2007. DOI: 10.1109/TWC.2007.348343
- [21] Andreas F. Molisch, "Statistical Description of the Wireless Channel," *Wireless Communications*, IEEE, pp.69-99, 2011. DOI: 10.1002/9781119992806.ch5
- [22] M. Al-Sadoon, R .A. Abd-Alhameed, I. T. E. Elfergani, J. M. Noras, J. Rodriguez, S. M. R. Jones, "Weight Optimization for Adaptive Antenna Arrays Using LMS and SMI Algorithms," *WSEAS Transactions on Communications*, vol. 15, pp. 206-214, 2016.
- [23] B. S. Basha, and M. M. Ismail, "Study and Analysis of Beamforming Algorithm between LMS and SMI," *Journal of Communications*, vol. 17, no. 6, pp. 472-477, Jun 2022.
- [24] M. H. Alsharif, R. Nordin, M. M. Shakir and A. M. Ramly, "Small cells integration with the macro-cell under LTE cellular networks and potential extension for 5G," *Journal of Electrical Engineering and Technology*, vol. 14, no. 6, pp. 2455-2465, 2019. DOI: 10.1007/s42835-019-00173-2

Chapter 4

Conclusion

OFDM systems continue to play an important role in 5G and the next generation 6G, due to their advantages of high spectrum utilization and resistance to multipath interference. However, there are many problems with the practical application of OFDM systems, such as the performance suffering greatly under high Doppler shift conditions under high-speed mobile environments or under conditions for interference in multi-user scenarios.

This paper mainly discusses two aspects of OFDM systems. On the one hand, the fast fading caused by high-speed mobile environments leads to a decrease in channel estimation accuracy, especially in the behind of the OFDM symbols. We use the machine learning method to improve the channel accuracy to overcome this problem. On the other hand, in multi-user scenarios, there is inter-user interference (IUI) for the desired user. To solve this problem, we propose a data expansion method to increase the number of samples and improve the accuracy of the weights based on the SMI of the array antenna algorithm.

Chapter 2 investigates regression CNN based on channel estimation to estimate CIS under a high-speed environment. Since the CSIs in the front of the packet are not the same as the ones on the back in a high-speed environment, a highly reliable

channel estimation method that can track time variations is needed. Conventional methods have proposed channel estimation methods using GRNN. However, when sharp channel fluctuations occur from the first half of the communication packet, the one-dimensional training data using DFCE in the time domain of the conventional method is erroneous. Furthermore, the channel estimation accuracy has become degraded. In fact, channel response has the time domain and the frequency domain, so it can be considered as two-dimensional data like an image. Therefore, the proposed method considers the relationship between the time and frequency domains and uses a regression CNN, which can extract the characteristics of two-dimensional data, to perform accurate channel estimation. In addition, by learning various channel data in advance, the amount of iterative operations can be decreased. Simulation results show that the BER characteristics can be significantly improved even in high-speed moving environments.

In Chapter 3, a weight estimation method based on the beamforming of array antennas has been proposed to overcome the IUI problem. The SMI method is well known as a weight estimation method for array antennas to perform beamforming. However, this method has problems with low interference suppression performance and high computational complexity since the weights are calculated for each OFDM subcarrier. The conventional method has proposed to increase the number of samples based on an adaptive grouping to improve the accuracy of the weights. However, since this method requires estimation of SNR and the number of samples is extended only in the frequency domain, the accuracy of the weights is insufficient and the computational complexity is greatly increased. Therefore, an algorithm that can improve the interference suppression performance with low computational complexity needs to be considered. In the proposed method, we use subcarrier grouping and decision feedback data to extend the number of samples in frequency and time domains. In addition, the LMS method is used to reduce

the computational complexity. The BER characteristics are improved with lower computational complexity compared to the conventional methods.

Acknowledgments

I would like to express my sincere gratitude to my supervisor, Prof. Ahn, for his kind care and patient guidance, encouragement and motivation throughout my graduate life at Chiba University. I have learned a lot from his rigorous scientific thinking, generous personality, conscientious work ethic, and his enthusiasm for education. These experiences are precious assets of my lifetime, and they will accompany me forever. I would like to express my utmost respect and heartfelt gratitude to my teacher once again.

I would also like to express my gratitude to Associate Professor K. Maruta from the Tokyo University of Science for his encouragement and for teaching me how to overcome the difficulties in my research.

I would like to thank all the faculty members of the Graduate School of Engineering group for providing me with an excellent education and research environment. I would like to thank Professor H.Sekiya and Associate Professor K.Nguyen for carefully reading my thesis and providing me with meticulous suggestions. I would also like to thank Ms. Endo and Ms. Namba for their patient guidance.

I would like to thank Assistant Professor S. Kojima from the University of Tokyo for his help and his valuable suggestions.

I wish to thank Mr. Wang, Mr. Toyama, Mr. Yamashita, Mr. Nagasato, Mr. Takehana, and Mr. Mano for their discussion and contributions to my work. I also would like to thank Mr. Miyamoto, Mr. Nishibe, Mr. Shibakura, Mr. Ito, Mr.

Kaihatsu, Mr. Nakano, Mr. Takemoto, Mr. Tamura, Mr. Ueno, and Mr. Fang for their discussion and support. Finally, I would like to express my gratitude to my parents, aunt and wife for their support.

I want to thank my cats, Haru, Chacha, and Boruta, for their company.

List of Related Papers

Journal Paper

- [1] Shun Kojima, He He, Kazuki Maruta, and Chang-Jun Ahn, “Generalized Regression Neural Network based Fast Fading Channel Tracking using Frequency-Domain CSI Smoothing,” *IEEE Access*, vol.90, pp.142425-142436, October 2021. DOI: 10.1109/ACCESS.2021.3121399
- [2] He He, Shun Kojima, Takaki Omura, Kazuki Maruta, and Chang-Jun Ahn, “Generalized Regression Neural Network based Channel Identification and Compensation Using Scattered Pilot,” *Radioengineering*, vol.30, no.4, pp.695-703, December 2021. DOI: 10.13164/re.2021.0695
- [3] He He, Shun Kojima, Kazuki Maruta, and Chang-Jun Ahn, “Adaptive Zero-Padding with Impulsive Training Signal MMSE-SMI Adaptive Array Interference Suppression,” *IEICE Transactions on Fundamentals of Electronics, Communications and Computer Sciences*, vol. E106-A, no. 4, pp. 674 - 682, Apr. 2023. DOI: <https://doi.org/10.1587/transfun.2022EAP1070>
- [4] He He, Jun-Han Wang, Shun Kojima, Kazuki Maruta, and Chang-Jun Ahn, “Data-aided weight with subcarrier grouping for Adaptive Array Interference Suppression,” *Journal of Communications Software and Systems*, vol. 18, no. 4, pp. 343-349, Dec. 2022. DOI: 10.24138/jcomss-2022-0109

- [5] He He, Jun-Han Wang, Shun Kojima, Kazuki Maruta, and Chang-Jun Ahn, “Regression CNN based Fast Fading Channel Tracking using Decision feedback channel estimation,” *Journal of Signal Processing*, vol. 27, no. 3, pp. 343-449, May. 2023. DOI:<https://doi.org/10.2299/jsp.27.49>.

International Conference Paper

- [1] He He, Shun Kojima, Kazuki Maruta, and Chang-Jun Ahn, “GRNN based Channel Estimation using Scattered Pilot and RBF Interpolation,” *Proc. International Conference on Emerging Technologies for Communications (ICETC2020)*, December 2020. DOI: 10.34385/proc.63.O1-2
- [2] He He, Shun Kojima, Kentaro Yonei, Kazuki Maruta, and Chang-Jun Ahn, “Variable Frame Splitting for Polar Coded MIMO E-SDM in Fast Fading Channel,” *Proc. IEEE 94th Vehicular Technology Conference (VTC 2021 - Fall)*, pp. 1-5, Virtual, September. 2021. DOI:10.1109/VTC2021-Fall52928.2021.9625224
- [3] He He, Shun Kojima, Kazuki Maruta, and Chang-Jun Ahn, “Data-aided weight with subcarrier grouping for Adaptive Array Interference Suppression,” *2022 IEEE International Conference on Consumer Electronics-Asia (ICCE-Asia)*, pp. 1-5, Yeosu, Korea, Nov. 2022. DOI: 10.1109/ICCE-Asia57006.2022.9954703.
- [4] Koji Nishibe, Takanori Shibakura, Koki Miyamoto, He He and Chang-Jun Ahn, “Novel IQ Imbalance Compensation Method for MIMO-OFDM Systems,” *2022 IEEE International Conference on Consumer Electronics-Asia (ICCE-Asia)*, pp. 1-4, Yeosu, Korea, Nov. 2022. DOI: 10.1109/ICCE-Asia57006.2022.9954703.

Domestic Conference Paper

- [1] 赫赫, 大村高輝, 丸田一輝, 安昌俊, “分散パイロット配置及びRBF補間を用い

た GRNN チャネル推定,” 2020 年電子情報通信学会総合大会, B-5-38, 2020 年 3 月.

[2] 小島駿, 赫赫, 王君ハン, 丸田一輝, 安昌俊, “敵対的生成ネットワークによる受信信号データセットの拡張,” 2022 年電子情報通信学会ソサイエティ大会, B-5-9, 2022 年 9 月.

[3] 田村幸佑, 小島駿, 赫赫, 丸田一輝, 安昌俊, ”GAN によるドップラーシフトに堅牢なデータセットの拡張,” 2023 年電子情報通信学会, 総合大会, B-5-5, 2023 年 3 月.

Award and Grant

[1] IEEE VTS Tokyo/Japan Chapter 2021 Young Researcher ’ s Encouragement Award

[2] IEEE ICCE-Asia 2022 Best Paper Award Gold Prize